Economic Geology
Vol. 84, 1989, pp. 506–528

Geochemical Modeling of Steady State Fluid Flow and Chemical Reaction during Supergene Enrichment of Porphyry Copper Deposits

JAY JAMES AGUE* AND GEORGE H BRIMHALL

Department of Geology and Geophysics, University of California, Berkeley, California 94720

Abstract

In this study motivated by detailed field work and laboratory analysis, we numerically simulate the supergene enrichment of porphyry copper deposits. We utilize a new program developed to model simultaneously advective solute transport in variably saturated porous media and chemical fluid-rock interactions incorporating mineral dissolution kinetics. Field and laboratory analytic and mineralogic data from supergene enrichment systems at Butte, Montana, and Ok Tedi, located in western Papua New Guinea, are used to provide geochemical, lithologic, and hydrologic initial and boundary conditions required for geologically relevant modeling.

We have simulated the weathering and supergene enrichment of porphyry copper potassium silicate proto-ore or "protore" containing disseminated pyrite and chalcopyrite in a one-dimensional, vertically oriented flow region under steady flow conditions for a total model time of about 12,000 yr. During this time primary chalcopyrite dissolves completely from the leached and blanket zones, pyrite is destroyed in the leached zone, and magnetite dissolves from the entire flow region. We therefore investigate both supergene enrichment processes and the response of the system to complete dissolution of a protore reactant.

Computed mineral assemblages are generally in excellent agreement with those observed in natural systems. Although copper is remobilized in the simulation by leaching above the model ground-water table and reprecipitation below it, the resulting differentiated weathering profile is chemically closed with respect to copper. This is because nearly all of the transported copper is fixed below the ground-water table by secondary sulfide precipitation. Therefore, an important conclusion to be drawn from the modeling is that in natural oxidative weathering, vertical copper fluxes out of supergene systems are probably negligible even over extremely long periods of geologic time. These theoretical results confirm earlier calculations of amounts of erosion and erosion rates, and reconstructions of paleotopography assuming copper mass balance in regions of vertical fluid flow (Brimhall et al., 1985; Alpers and Brimhall, 1988, 1989). Sulfur, in contrast, is mobile during the simulation and significant quantities of sulfate leave the flow region with time. Modeling results indicate that the dominant source of sulfur for secondary copper sulfide mineral formation in the enrichment blanket is the preexisting protore sulfides, not electrochemical reduction of the sulfate transported out of the leached zone. The numerical simulation demonstrates that oxygen fugacity is the primary control governing the nature and extent of low-temperature reequilibration of the fossil magmatic-hydrothermal system in the near-surface weathering environment.

Introduction

THE importance of supergene oxidation and transport of metals in the enrichment of base metal ore deposits exposed in the weathering environment has long been appreciated (cf. Emmons, 1918; Locke, 1926; Bateman, 1950). In broad terms, supergene enrichment requires hydrochemical differentiation by near-surface weathering processes in which ground-water transports metals from a source region or leached zone to a locus of enrichment or blanket zone where these ions are reprecipitated as secondary ore compounds. Particular attention has been focused on the supergene ores of copper due to their global economic significance and the dramatic extent to which metals and sulfur are remobilized during oxidative weathering. In addition, lateritic weathering of mafic-ultramafic rocks (cf. Elias et al., 1981; Golightly, 1981) may cause strong supergene enrichment of economically important metals such as nickel (e.g., Brimhall and Dietrich, 1987).

Previous studies of oxidative weathering of copper sulfide deposits have largely been concerned with deducing the original spatial distribution of primary high-temperature sulfide assemblages based on relict sulfides and limonite mineralogy in gossans (cf. Locke, 1926; Blanchard, 1968; Lowell and Guilbert, 1970; Loghry, 1972; Blain and Andrew, 1977; Titley and Beane, 1981; Anderson, 1982). More recently it has been shown that constitutive mass balance *relation-*

* Present address: Department of Geology and Geophysics, Yale University, P.O. Box 6666, New Haven, Connecticut 06511.

0361-0128/89/920/506-23$3.00

ships which take into account variations in rock chemistry, density, volume, porosity, and primary vertical geochemical zoning may be used to estimate quantitatively the amounts of erosion, erosion rates, and volumetric strain in weathering systems and also to assess the relative importance of residual versus supergene enrichment processes (Brimhall et al., 1985; Brimhall and Dietrich, 1987; Alpers and Brimhall, 1988, 1989). In addition, regions where lateral (i.e., nonvertical) fluid flow has been important in the enrichment or depletion of metals may be identified and related to regional fault zones (Brimhall et al., 1985).

Although substantial progress has been made in understanding the varied geological, hydrological, and climatological controls which influence the nature and extent of supergene enrichment processes (cf. Emmons, 1918; Bateman, 1950; Peterson et al., 1951; Titley, 1978; Graybeal, 1982; Brimhall and Dietrich, 1987; Alpers and Brimhall, 1988, 1989), outstanding unanswered questions remain. For example, how do mineralizing fluid chemistry and precipitated mineral assemblages evolve as functions of time and position within the weathering environment? What are the dominant chemical species transported between the various weathering zones? What chemical changes occur in response to the immense decrease in oxidation potential attending the transition from the leached zone above the capillary fringe of the ground-water table to the enrichment zone below it? Which elements are quantitatively fixed within the enrichment zone and which are largely transported out of the weathering system? How accurate is the assumption that copper leached from above the ground-water table is quantitatively reprecipitated below? Do theoretical mass transport calculations support the use of reconstructions of paleotopography and paleoclimatic regimes (cf. Brimhall et al., 1985; Brimhall and Dietrich, 1987; Alpers and Brimhall, 1988) based upon mass balance principles?

Because enrichment processes operate over geologic periods of time it is not possible to observe the entire hydrochemical evolution of a supergene orebody directly. Therefore, in order to address these questions, we have developed a numerical model which explicitly couples advective transport of chemical species in solution in both unsaturated and saturated porous media with irreversible thermodynamic calculation of fluid-rock interactions. Use of a coupled fluid flow-chemical reaction approach allows us to treat the geochemically diverse weathering zones developed above and below the ground-water table as a single integrated supergene system.

We attempt to use theoretical first principles to simulate supergene solute transport and fluid-rock interactions. However, it must be emphasized that only by careful comparison of model results with observations in natural systems can we conclude that the model has geologic relevance. Sulfur transport processes offer a critical test of the theoretical modeling approach because we now know much about the geochemistry, hydrology, mineralogy, and petrology of these highly accessible supergene systems. Under such direct comparisons between nature and model results, we can establish what constitutes an acceptable theoretical simulation.

In this paper we numerically model weathering and supergene enrichment of porphyry copper potassium silicate proto-ore or "protore" containing disseminated copper and iron sulfides using one set of representative initial and boundary conditions (Fig. 1). The protore mineralogy corresponds to the pre-Main Stage rocks within the Butte district of Montana (Meyer, 1965; Meyer et al., 1968; Brimhall, 1977, 1979, 1980) which are, in general, typical of many porphyry copper potassium silicate protores worldwide. We have carried out the weathering simulations for sufficiently long model times such that primary chalcopyrite, pyrite, and magnetite completely dissolve from the leached zone. This allows us to study the geochemical evolution of the supergene system from the ore-forming stage in which leaching, transport, and reprecipitation of copper takes place, to the point where all primary copper and iron-bearing sulfides and oxides have been destroyed in the leached zone, thus signaling the end of the secondary ore-forming episode under steady flow conditions.

In order for the results of the calculations to be as realistic as possible, it is essential that measurements of fundamental variables such as rock porosity and

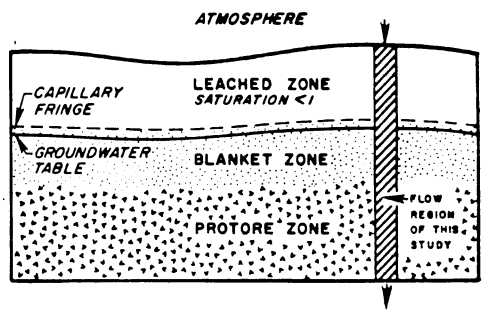

FIG. 1. Cross section through a supergene enrichment system. Downward-moving ground waters transport Cu^{+2} and other ions from the oxidizing leached zone, in which rock voids are filled with both air and water, below the capillary fringe of the ground-water table. Here, precipitation of secondary sulfides and other minerals occurs in the enrichment blanket during supergene enrichment. The stable protore is little modified during weathering. The shaded box schematically illustrates the one-dimensional flow region modeled in this study. Vertically oriented arrows indicate the direction of fluid movement through the flow region (cf. Fig. 2). The protore is quartz monzonite with K silicate alteration and pyrite-chalcopyrite mineralization. The blanket zone has additional secondary copper minerals chalcocite and covellite.

meteoric water redox state in natural systems be used as input into the model. To this end we have utilized field and laboratory mineralogic and analytic data from the porphyry copper-molybdenum deposit at Butte, Montana, and the Ok Tedi porphyry copper-gold deposit located in western Papua New Guinea to constrain initial and boundary conditions in the numerical simulations. The Butte district has been extensively studied (cf. Meyer et al., 1968; McClave, 1973; Brimhall, 1977, 1979, 1980; Brimhall and Ghiorso, 1983; Brimhall and Ague, 1988) and critical rock properties necessary for fluid flow modeling have been measured on samples from this deposit by Cunningham (1984). The Ok Tedi weathering system (cf. Bamford, 1972) is important in that it provides an ideal field location in which to observe supergene enrichment processes operative in potassium silicate protore today.

Previous Modeling Studies

In general, two distinct computational schemes have been employed in the past to model numerically the coupled fluid flow and chemical reaction in geologic environments. One method involves simultaneous solution for every time step of all equations describing solute transport and irreversible thermodynamics by implicit finite difference or finite element techniques. The other explicit-coupling approach, utilized in this study, employs a sequential solution technique in which the solute transport and chemical thermodynamic equations are solved separately for each time step. The latter approach has the advantage of being able to model complex geologic systems with reasonable computational efficiency given the current state of computer technology.

Previous geochemical modeling of supergene copper enrichment has focused largely upon individual environments within the weathering system, particularly the leached zone (cf. Cathles and Apps, 1975; Braithwhite, 1976; Cathles, 1979; Bladh, 1982). Noteworthy exceptions include the explicitly coupled approach used by Cunningham (1984) in the simulation of incipient stages of ore formation, and by Narasimhan et al. (1986b) who focused on redox phenomena attending supergene copper transport. In spite of these efforts, the varied interrelationships which evolve between the leached zone, enrichment blanket, and protore portions of the weathering profile during and after the supergene ore-forming event remain to be investigated numerically.

Important progress has been made in studies of other metasomatic processes using a variety of computational schemes. For example, Garven and Freeze (1984) demonstrated that the flow of gravitationally driven oil field brines through carbonate rocks may produce Mississippi Valley-type Pb-Zn mineralization. However, a critical difference between the approach of Garven and Freeze (1984) and that utilized in the present study is that we perform the full set of calculations for fluid flow and irreversible thermodynamics over each time step throughout the flow region. This is in contrast to Garven and Freeze (1984) who carried out the chemical reaction computations only during the final part of the simulation when the mineralizing fluids reach the site of ore formation. Lichtner (1985) has developed a comprehensive mathematical formulation and implicit finite difference algorithm to solve simultaneously the governing equations of fluid flow and chemical reaction. This approach, while elegantly treating mass transfer in metasomatic systems, has the disadvantage of being computationally inefficient for problems involving more than four or five chemical elements. Other workers who have utilized implicit finite difference or finite element solution techniques include Rubin and James (1973), Jennings et al. (1982), and Miller and Benson (1983). Examples of explicitly coupled models developed to study various aspects of multiple species chemical transport in ground-water systems include those of Dutt et al. (1972), Wierenga et al. (1975), Grove and Wood (1979), Schulz and Reardon (1983), Cederberg (1985), and Narasimhan et al. (1986a, b).

Computational Approach

In order to model the supergene enrichment system consisting of leached zone, blanket zone, and protore as an integrated hydrochemical system, we have developed an explicitly coupled advective solute transport-chemical reaction program. Although we focus here on a one-dimensional problem (Fig. 1), the approach taken is general and can be extended to two or three dimensions. The program TRUST (Narasimhan and Witherspoon, 1977; Narasimhan and Witherspoon, 1978; Narasimhan et al., 1978) is utilized to describe fluid flow owing to its ability to handle one-, two-, or three-dimensional flow through variably saturated porous media of widely varying physical properties and geometries. The ability to model fluid flow under different conditions of water saturation is critical because saturation is less than one in the leached zone, whereas the blanket and protore zones are fully saturated (Fig. 1). The highly versatile EQ3NR and EQ6 programs (Wolery, 1979, 1983) compute the distribution of aqueous species in a given fluid, and perform calculations of fluid-rock interactions, respectively. All thermodynamic computations have been carried out at 25°C and 1 bar. The fluid flow and chemical reaction calculations are coupled using an advective solute transport algorithm. Diffusion and hydrodynamic dispersion have been neglected because they are probably of second-order importance to advection as processes of solute transport. The numerical formulation and execution pro-

cedure employed in the coupled fluid flow-chemical reaction program are presented in detail in the Appendix.

Properties of the Flow Region

Here we discuss the critical hydrologic, geochemical, and mineralogic properties of the model weathering system. We have not run multiple simulations to investigate the effects of altering the values of any of the model initial and boundary conditions. Instead, our goal is to simulate the weathering and supergene enrichment of a common porphyry copper ore type, utilizing one set of representative initial and boundary conditions, in order to trace the geochemical evolution of a "typical" enrichment system.

Hydrologic properties

We model coupled steady state fluid flow and chemical reaction in a vertical, one-dimensional flow region (Fig. 1), in which fluid motion is governed by Darcy's law. For the purposes of coupled calculation, the flow region has been subdivided into five volume elements, each of which is 30 m long and 1 m^2 in cross section (Fig. 2). This subdivision provides sufficient spatial resolution for our study of oxidative weathering processes and allows the fluid flow and chemical reaction calculations to be completed in a reasonable amount of time.

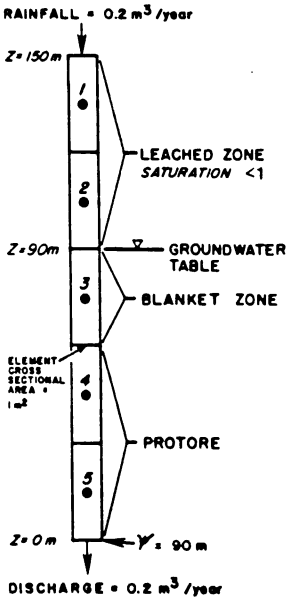

FIG. 2. Supergene enrichment flow region. Volume elements 1 and 2 lie above the ground-water table and represent the leached zone. Saturation states of elements 1 and 2 are 0.68 and 0.74, respectively. Volume element 3 is fully saturated and evolves into the enrichment blanket during the simulation. Volume elements 4 and 5 represent the stable protore. Black dots within volume elements are nodal points (see Appendix). Note that the large size of the volume elements does not permit resolution of the capillary fringe. Boundary conditions are the rainfall input and the constant pressure head boundary at the base of the system.

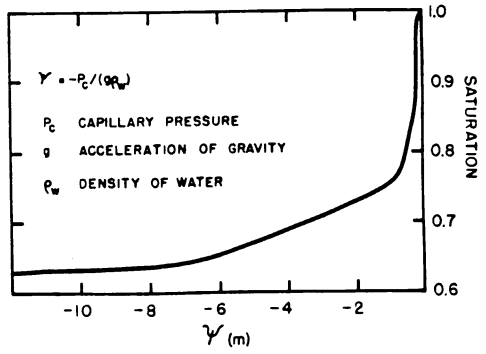

FIG. 3. Saturation versus pressure head curve used in this study. Average of measurements made by Cunningham (1984) on eight samples from the supergene enrichment system at Butte, Montana. Relation between pressure head and capillary pressure is also shown.

The physical properties of the rocks which are of critical importance in simulating fluid flow are porosity (n), saturation as a function of piezometric head (ψ), and permeability. Cunningham (1984) measured the porosity of samples from two drill holes in the Butte district. The average value of porosity which he obtained, 0.12, is used in this study. Values of rock saturation as a function of ψ are necessary to evaluate saturation states within the unsaturated zone of the flow region. The values used in this study were measured by Cunningham (1984) on samples from the Butte district (Fig. 3). We have not measured sample permeability and therefore a representative value of 10^{-14} m^2 (Brace, 1980) has been used.

The boundary conditions imposed on the flow region simulate the input of rainfall into the subsurface and establish the level of the ground-water table (Fig. 2). Rainfall is input into the top of the flow region at a moderate rate of 0.2 m^3/yr. The dissolved solute content of the rainwater used in the simulation is from Bladh (1982) (Table 1). The pH of the input rainwater is 6.2 (Table 1). This value is the average of pH measurements we made in the field on meteoric waters

TABLE 1. Rainwater Composition (moles/l)

Al	1.0×10^{-8}
Ca	2.5×10^{-6}
Cl	1.0×10^{-4}
Cu	2.0×10^{-8}
Fe	1.0×10^{-12}
K	8.0×10^{-6}
Na	1.6×10^{-5}
$SiO_{2(aq)}$	1.4×10^{-5}
S	6.0×10^{-6}
pH	6.2

Solute concentrations from Bladh (1982); rainwater pH measured in this study at Ok Tedi

at Ok Tedi. The level of the ground-water table has been fixed by imposing a constant 90-m boundary potential at the base of volume element 5. Because rainfall is input at a constant rate of 0.2 m^3/yr into the top of the system, in order to keep the lower boundary potential constant at 90 m, the flow region must drain, also at a rate of 0.2 m^3/yr. Thus, these two boundary conditions work in concert to produce steady, one-dimensional flow. The Darcy velocity of the fluid is 6.3×10^{-9} m/s. No attempt has been made here to relate changes in volume due to mineral precipitation and dissolution to changes in porosity and permeability, primarily because such relationships are currently very poorly understood in shallow weathering environments. Therefore, flow remains steady throughout the course of the simulations.

Under these boundary conditions, volume elements 1 and 2 remain unsaturated and therefore represent the leached zone of the weathering copper porphyry (Fig. 2). In contrast, volume elements 3, 4, and 5 remain fully saturated throughout the simulation. Secondary copper sulfides produced during supergene enrichment precipitate within volume element 3, the blanket element. It should be pointed out here that the volume elements comprising the flow region are too large to resolve the capillary fringe in detail. Thus, in the simulation the top of the capillary fringe corresponds to the top of volume element 3. Volume elements 4 and 5 are little modified during the simulation and therefore represent the stable protore.

In nature, annual climatic cycles may produce small-scale fluctuations in the level of the ground-water table. Furthermore, long-term climatic changes may influence dramatically the degree of enrichment in dynamic supergene systems (Alpers and Brimhall, 1989). However, in the simulation effort described herein, we model the case in which the level of the ground-water table remains constant. We do this because a flow region containing a nonfluctuating ground-water table is the simplest possible supergene environment to study and serves as a starting point for the future consideration of more complex hydrologic systems.

Geochemical and mineralogical properties

The starting rock mineralogy utilized in the simulations is that of the pre-Main Stage lithology within the Butte district of Montana (cf. Meyer, 1965; Brimhall, 1977, 1979, 1980) which contains on average 20 percent K-feldspar, 34 percent plagioclase (An_{30}), 21 percent quartz, 10 percent biotite, 6 percent muscovite (sericite), 4 percent pyrite, 2 percent chalcopyrite, and 2 percent magnetite by volume. The sericite forms during high-temperature alteration and occurs replacing igneous minerals such as plagioclase. Chlorite, rutile, and zircon may also occur, but since these phases probably do not influence supergene enrichment processes to any significant degree, they have been omitted from the model protore. No solid solution between the albite and anorthite components of plagioclase has been considered and therefore albite and anorthite have been modeled as separate phases with modal percentages of 24 and 10 percent, respectively. The biotite is assumed to be pure annite for modeling purposes.

This protore assemblage formed originally at high temperatures (600°–650°C) under magmatic-hydrothermal conditions (Brimhall, 1977) and has not been modified by circulation of later highly acid, sulfate- and copper-rich fluids of the advanced argillic alteration stage generated in response to meteoric water influx into the cooling porphyry system (cf. Brimhall and Ghiorso, 1983). The pre-Main Stage protore is considered here because a number of reactant phases which can enter into important acid and redox buffering relationships, such as biotite, are completely destroyed during advanced argillic alteration. Thus, modeling of supergene enrichment of pre-Main Stage protore is a thermodynamically more well-constrained problem than modeling weathering in a protore strongly affected by advanced argillic alteration.

The redox state of waters in the leached zone above the capillary fringe of the ground-water table is a fundamental control on the nature and rates of oxidative weathering in the unsaturated zone. Although the diffusion of oxygen gas through variably saturated porous media can be calculated (cf. Troeh et al., 1982), the oxygen content of the water in contact with the gas phase is much more difficult to assess. This is because the oxidation potentials of meteoric and near-surface waters in contact with the atmosphere are always significantly lower than the calculated potential for the half-reaction describing equilibrium between water and oxygen at atmospheric concentrations (cf. Baas Becking et al., 1960; Garrels and Christ, 1965; Krauskopf, 1979). This discrepancy was addressed by Sato (1960) who postulated that oxidation reactions involving oxygen may have complicated mechanisms whose rates are governed largely by kinetically slow steps in which H_2O_2 may be important. In view of these complexities, we utilize Eh-pH values of meteoric and near-surface waters which we have measured in the field at the Ok Tedi copper-gold deposit in Papua New Guinea in order to place meaningful constraints on the oxidation potential of waters in the unsaturated zone (Fig. 4). Ok Tedi is an ideal deposit in which to make such measurements because supergene enrichment of potassium silicate protore is actively occurring there today. On average, the measurements correspond to oxygen fugacities on the order of 10^{-35} which agree well with the measurements made by Sato (1960) on waters in sulfide-bearing leached caps (Fig. 4). Based on these data from natural systems, we have fixed the oxygen fugacity in volume

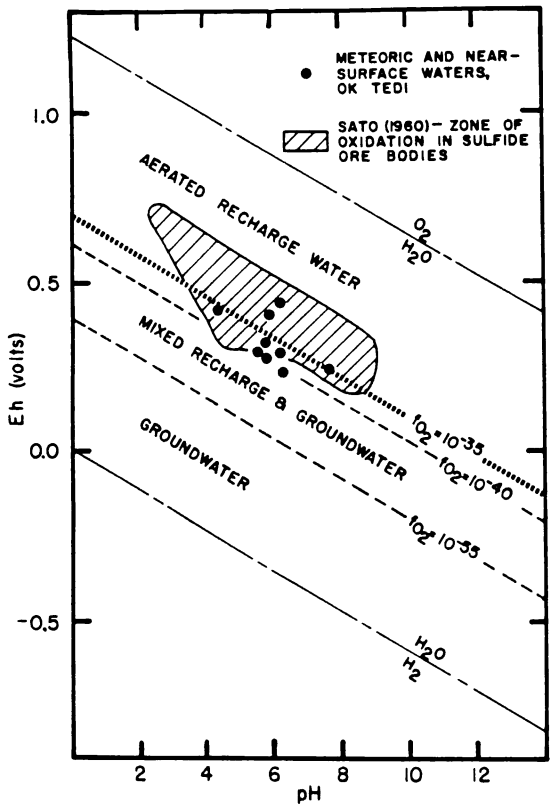

FIG. 4. Eh-pH conditions measured in meteoric water, soils, and the upper portion of the leached zone at Ok Tedi, and other oxidizing sulfide systems from Sato (1960). Average f_{O_2} conditions of these waters are 10^{-35}. Fields of aerated waters, mixed waters, and ground waters from Garrels and Christ (1965).

elements 1 and 2 at a constant value of 10^{-35} throughout the simulation. Below the water table in volume elements 3, 4, and 5, the redox state is determined by the buffering mineral assemblages in the rocks.

The remaining geochemical boundary conditions to be addressed are the dissolution rates of the protore reactants. Consideration of protore mineral dissolution kinetics is essential in order to facilitate the critical linkage of fluid flow and chemical reaction calculations in model time. We utilize a linear (far from equilibrium) kinetic rate law of the form:

$$R_{rct} = k_{rct}s_{rct}, \quad (1)$$

where k_{rct} = dissolution rate constant of reactant rct [moles/(L^2t)], rct = a mineral reactant, R_{rct} = dissolution rate (R) of reactant rct [moles/t], and s_{rct} = reactive surface area of reactant rct [L^2]. The use of more complex expressions is presently unwarranted owing to uncertainties in both mechanisms of dissolution and values of rate constants for a number of important minerals. The surface area term in equation (1) has been estimated geometrically assuming that the mineral grains in the rock are cubes with an edge length of 2 mm, which corresponds to the average grain size measured in pre-Main Stage protore. Because there is currently no quantitative understanding of changes in mineral reactive surface areas over long periods of time in weathering rock masses, we have for modeling purposes kept s_{rct} constant for all reactants throughout the simulation. Values of rate constants are summarized in Table 2 and discussed in detail below.

For feldspars, sufficient experimental data exists such that the pH dependence of the rate constant may be established (cf. Busenberg and Clemency, 1976; Holdren and Berner, 1979; Lasaga, 1984). The appropriate linear rate expression is:

$$R_{rct} = k'_{rct}a_{H^+}^{n_{H^+}}s_{rct}, \quad (2)$$

where a_{H^+} = activity of aqueous hydrogen ion, k'_{rct} = operational rate constant of reactant rct [moles/(L^2t)], and n_{H^+} = dissolution rate order with respect to aqueous hydrogen ions. The k' and n_{H^+} values for

TABLE 2. Dissolution Rate Constants of Protore Reactants

Reactant	pH range	k[moles/cm²/s]	k'[moles/cm²/s]	n_{H+}	Source
K-feldspar	<2.8		2.0×10^{-13}	−1.0	1
Albite, Anorthite	>2.8		3.2×10^{-16}	0.0	
Quartz	All	1.6×10^{-18}			4
Annite, muscovite	All	2.4×10^{-18}			5
Pyrite	<2.0	See text			3
	>2.0	4.0×10^{-15}			6
Chalcopyrite	<2.0	See text			2
	>2.0	4.0×10^{-15}			6
Magnetite	All	2.0×10^{-15}			6

Data sources: 1, Helgeson et al. (1984); 2, Gagen (1987); 3, McKibben and Barnes (1986); 4, Murphy (1985); 5, Wood and Walther (1983); 6, estimated in this study

feldspars in Helgeson et al. (1984) are utilized here (Table 2). Because in the natural protore, albite and anorthite occur as components in sodic plagioclase, we have for simplicity used the k′ and n_{H^+} values of albite to represent both albite and anorthite dissolution in the model. Quartz dissolution may be relatively independent of pH, at least in the moderately acid to neutral pH range (cf. Rimstidt and Barnes, 1980; Murphy, 1985) and we have therefore used a single rate constant to describe dissolution of this phase. Owing to the lack of experimental data for the dissolution rates of annite and muscovite, we have employed the method of Wood and Walther (1983) to estimate the rate constants of these phyllosilicates.

The dissolution rates of sulfides, particularly pyrite, have been extensively studied at low pH (cf. Nordstrom, 1982; Wiersma and Rimstidt, 1984; McKibben and Barnes, 1986), but there is a paucity of kinetic data at pH values higher than 2 for the low dissolved oxygen contents present in subsurface waters.

We may write the following overall reaction to describe pyrite oxidation at the relatively low dissolved oxygen concentrations present in the fluids considered in this study:

$$FeS_2 + 14Fe^{+3} + 8H_2O \rightarrow 15Fe^{+2} + 2SO_4^{-2} + 16H^+. \quad (3)$$

In the pH range of 1 to 2, McKibben and Barnes (1986) put forth the following expression for k_{pyrite} which is dependent upon the molarities of Fe^{+3} and H^+ in solution:

$$k_{pyrite} = -10^{-9.74}(M_{Fe^{+3}})^{0.5}(M_{H^+})^{-0.5}. \quad (4)$$

For chalcopyrite, the overall oxidation reaction may be written as (Gagen, 1987):

$$CuFeS_2 + 16Fe^{+3} + 8H_2O \rightarrow Cu^{+2} + 17Fe^{+2} + 2SO_4^{-2} + 16H^+. \quad (5)$$

At a pH of 2, Gagen (1987) measured the rate of reaction of chalcopyrite with ferric iron. Using this data, the change in moles of chalcopyrite with time may be expressed as:

$$\frac{dn_{cp}}{dt} = \frac{1}{16}(1.5 \times 10^{-3})(M_{Fe^{+3}})^{0.94}A, \quad (6)$$

where n_{cp} represents moles of chalcopyrite and A is the ratio of reactive surface area to the mass of the aqueous solution.

At pH values higher than 2, the values of sulfide dissolution rate constants are much more poorly constrained owing to a lack of experimental data. However, Braithwaite (1976) developed expressions describing the rate of chalcopyrite dissolution in mill tailings piles over a range of pH values. Cunningham (1984), using the data and equations of Braithwaite (1976), calculated that the rate constant for chalcopyrite ranged from 4×10^{-14} moles/cm^2/s to 4×10^{-16} moles/cm^2/s between pH 2 and pH 6. For simplicity, owing to the current scarcity of information pertaining to sulfide dissolution at higher pH values, we have set the rate constant for both pyrite and chalcopyrite at a representative value of 4×10^{-15} moles/cm^2/s for pH values greater than 2. This is roughly an order of magnitude greater than the largest silicate dissolution rate constants. Preliminary results from chalcopyrite dissolution experiments which we have carried out indicate that in the pH range of 4 to 7, the rate constant value of 4×10^{-15} moles/cm^2/s reproduces the experimental results within a factor of 1.5 using a linear kinetic rate law.

We are aware of no published studies of magnetite dissolution rates which are directly applicable to the oxidizing supergene environment. In view of the fact that magnetite is highly unstable and is only preserved in leached zones as relict grains encased in stable phases such as quartz (cf. McClave, 1973), we have approximated magnetite dissolution using a relatively large rate constant of 2×10^{-15} moles/cm^2/s. This is half the value of the rate constant used for pyrite and chalcopyrite at pH values greater than 2

Owing to a lack of experimental data, all phases which precipitate during the simulation are assigned a dissolution rate of 1×10^{-11} moles/s for simplicity. This rate is the average of the protore reactant dissolution rates. In addition, the precipitation kinetics of almost all of the minerals relevant to this study are currently not well understood. Therefore, mineral precipitation kinetics are not considered in the model.

Utilizing the initial and boundary conditions discussed above, steady state geochemical behavior may occur at various model times during the weathering simulation. Steady state is attained when fluid fluxes, fluid compositions, and amounts of minerals dissolved and precipitated are constant, within numerical precision, from one time step to the next. Steady state behavior is perturbed whenever a protore reactant, such as pyrite or chalcopyrite, dissolves completely from one or more zones within the simulated enrichment profile. The model steady states are relevant and useful approximations of complex natural irreversible weathering processes. Further details regarding steady state computations are provided in the Appendix.

Because of the large uncertainties in the values of some of the rate constants, the calculated model times are interpreted to be accurate to within about one order of magnitude. However, the relative rates of dissolution of the various protore sulfides, oxides, and silicates, with respect to each other, are probably better constrained. Therefore we feel that the geo-

chemical evolution of the weathering system can be modeled with acceptable accuracy, even though considerable uncertainty still exists regarding the absolute time scale over which supergene processes operate.

Modeling Results

The equilibration of copper sulfide-bearing protore with oxygenated meteoric waters in the weathering environment is a complex process which, under appropriate geologic, hydrological, and climatological conditions may produce supergene copper deposits with metal grades as much as five times higher than the unweathered and unenriched protore (cf. Titley and Beane, 1981). We have modeled this process using the initial and boundary conditions discussed above for a total model time of about 12,000 yr. At different times within this 12,000-yr interval, the critical protore reactants chalcopyrite, pyrite, and magnetite dissolve completely from various weathering zones within the metasomatic system. We may therefore gain insights into the geochemical systematics of weathering during supergene copper enrichment and also investigate how the system may respond to the disappearance of protore minerals essential to the enrichment process such as chalcopyrite and pyrite. In analyzing the results of the simulation, we focus on the mineral assemblages which form through time, chemical element mobility in the weathering profile, and the chemical evolution of supergene fluids as they react with the pre-Main Stage protore.

In the discussion which follows we have, for ease of presentation, labeled important points in time in the simulation, corresponding to complete dissolution of a protore phase within one or more volume elements, with capital letters. Intervals of steady state behavior are labeled with numbers. At point A (6,170 years) chalcopyrite is destroyed in volume elements 1, 2, and 3. At point B (11,030 years) pyrite dissolves completely from volume elements 1 and 2. Point C (11,870 years) represents the disappearance of magnetite from all volume elements. Intervals of steady state behavior occur between these points in time. Steady state 1 (140–6,170 years) corresponds to leaching of primary sulfides in volume elements 1 and 2 and the formation of the chalcocite-covellite enrichment blanket in volume element 3. Steady state 2 (6,310–11,030 years) occurs between points A and B whereas steady state 3 (11,180–11,870 years) occurs in the time interval between points B and C. In steady state 4 (>12,010 years) all Fe^{+3}-bearing protore reactants have been destroyed in the leached zone. For clarity, geochemical results presented below for the leached, blanket, and protore zones are from volume elements 1, 3, and 5, respectively, unless otherwise noted. We do this because volume elements 1 and 2 are in general very similar throughout the simulation, as are volume elements 4 and 5.

Mineral assemblages

A direct way to assess the overall accuracy of the numerical simulation is to compare the stable mineral assemblages predicted by the model to those present in natural supergene enrichment systems. Beyond this, the numerical simulation can provide important information about when a given mineral phase is stable and also what conditions within the weathering environment promote its precipitation or dissolution. Stable minerals in the various weathering zones during steady states 1, 2, 3, and 4 are shown in Figure 5. In general, there is excellent agreement between the computed assemblages and those which may form in nature.

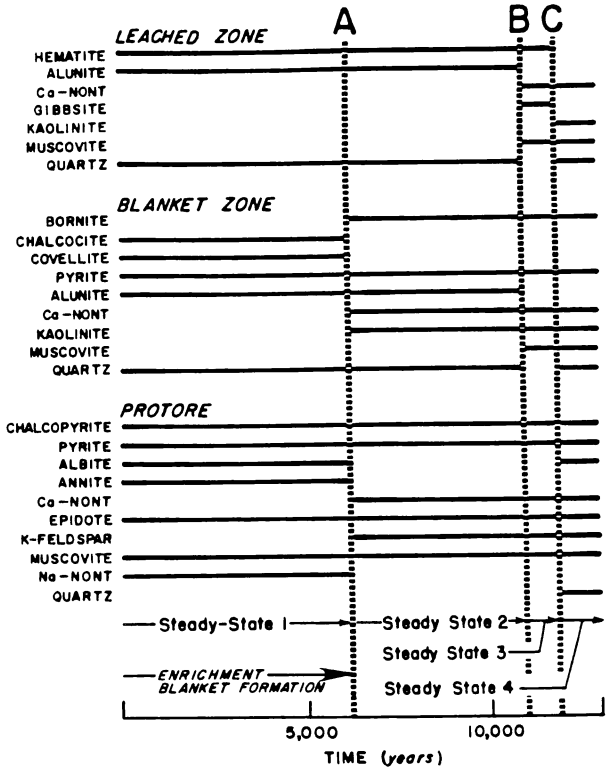

FIG. 5. Stable mineral assemblages over steady states 1, 2, 3, and 4 as a function of time. At point A (6,170 years) chalcopyrite disappears from the leached and blanket zones. At point B (11,030 years) pyrite dissolves completely from the leached zone. At point C (11,870 years) magnetite dissolves completely from the entire flow region. Steady states 1 (140–6,170 years), 2 (6,310–11,030 years), 3 (11,180–11,870 years), and 4 (>12,010 years) occur between these points. From the time a protore reactant dissolves, it takes approximately 140 years for the entire flow region to reach steady-state behavior. Minerals which precipitate and then redissolve during these 140-yr intervals are not shown for clarity. Nont = nontronite.

During the formation of the enrichment blanket over steady state 1, the stable product assemblage in the leached zone comprises hematite, alunite, and quartz. Alunite is a product of oxidative weathering in many sulfide orebodies (cf. Rye et al., 1988). Importantly, supergene and hypogene alunite may be dated radiometrically in order to trace the dynamic evolution of supergene systems (Alpers and Brimhall, 1988). Although the modeling results are in good agreement with natural assemblages (cf. Locke, 1926; Loghry, 1972; McClave, 1973; Alpers and Brimhall, 1989), goethite, an important constituent of many leached cappings, remains slightly undersaturated by approximately 2.5 kJ. In the simulations, hematite and goethite are considered to be pure phases and are related by the hydration reaction:

$$Fe_2O_3 + H_2O = 2FeO(OH). \quad (7)$$

The phase rule indicates that only one of these mineral phases is stable at a given temperature, pressure, and activity of water in the Fe_2O_3-H_2O system and this accounts for the presence of only hematite in the simulation.

However, in nature, the stability relations of hematite and goethite are considerably more complex (Berner, 1969, 1971; Schwertmann, 1985) and involve such factors as the Al content of the phases (cf. Schwertmann, 1985; Tardy and Nahon, 1985), their grain size (Langmuir, 1971, 1972), water activity, kinetic effects (Berner, 1969, 1971), solution pH (cf. Alpers and Brimhall, 1989), and the concentrations of other dissolved ions (cf. Torrent and Guzman, 1982). In fact, it is probable that the two phases form by different reaction mechanisms and are not directly related by equation (7). Given the very close thermodynamic stability of the two minerals (Berner, 1969, 1971) and the current uncertainties in their stability relations, the computed result of hematite production in the leached cap should be interpreted broadly as the formation of hematite and/or goethite. In addition, jarosite ($KFe_3(SO_4)_2(OH)_6$), which may occur in the leached zone overlying pre-Main Stage protore in the Butte district, is not precipitated during the simulation. However, its stability relationships with hematite, goethite, and alunite are complex and currently incompletely understood (cf. Nordstrom and Munoz, 1986; Alpers and Brimhall, 1989).

The product mineral assemblage in the leached zone remains unchanged after chalcopyrite dissolves completely from volume elements 1, 2, and 3 at point A. However, after pyrite is destroyed in the leached zone at point B, the mineral assemblage produced during weathering shows a marked change and comprises hematite, gibbsite, and "muscovite." In this case, the "muscovite" should be interpreted to be fine-grained sericite. A minor amount (about 0.2 vol %) of the clay mineral Ca nontronite ($Ca_{0.165}Fe_2Al_{10.33}Si_{3.67}O_{10}(OH)_2$) is also present. Even though substantial amounts of Ca are removed from the leached zone during oxidative weathering, the analyses of Cunningham (1984) from the Butte district show that 0.2 to 0.3 wt percent Ca may remain. The formation of a minor quantity of Ca-bearing clay in the simulation is consistent with natural leached zone Ca contents and observed mineralogy (cf. Cunningham, 1984).

After magnetite is dissolved from the flow region at point C, the leached zone product assemblage is dominated by kaolinite, and muscovite (sericite) formed through the hydrolysis of feldspars and micas. A small amount of Ca nontronite remains in the assemblage. Quartz is also stable. These results highlight the transition from acid weathering conditions, caused by the dissolution of chalcopyrite and pyrite, in which alunite, hematite, and quartz are stable, to conditions of less extreme pH where the weathering assemblage is dominated by silicate clay minerals.

In the blanket zone, the secondary copper sulfide assemblage produced during steady state 1 comprises chalcocite and covellite with a molar chalcocite/covellite ratio of about 0.2. This is in excellent agreement with the natural results of supergene enrichment of pre-Main Stage protore at Butte, Montana, in which the dominant secondary phase is covellite (McClave, 1973; Cunningham, 1984). It should be noted that in the context of the simulation, the formation of chalcocite (Cu_2S) should be interpreted to represent not only the formation of stoichiometric chalcocite, but also the other closely related phases with which it is typically found in nature such as digenite ($Cu_{1.70-1.74}Fe_{0.05-0.10}S$) and djurleite ($Cu_{1.934-1.965}S$). Chalcopyrite is unstable, consistent with petrographic observations which show that it is generally replaced by secondary sulfides at Butte, Montana, and elsewhere (cf. McClave, 1973; Alpers and Brimhall, 1989). Pyrite, quartz, and alunite are also stable within the enrichment blanket (cf. Alpers and Brimhall, 1988, 1989), whereas the feldspars, micas, and magnetite are not, again in good agreement with mineral assemblages in natural deposits (cf. Locke, 1926; Bateman, 1950; Titley, 1978).

After chalcopyrite dissolves from volume elements 1, 2, and 3 at point A, copper ions are no longer being transported into the blanket zone from the leached zone. During steady states 2, 3, and 4 the stable copper sulfide phase in the blanket zone is bornite, and a small amount of the chalcocite and covellite produced during supergene enrichment is converted to this phase for the remainder of the simulation. Kaolinite and Ca nontronite are stable after point A, and therefore these phases appear significantly earlier in the blanket zone than they do in the leached capping. Pyrite, alunite, and quartz continue to be stable

phases. After the disappearance of pyrite from the leached zone at point B, alunite is no longer stable whereas muscovite (sericite) is. Quartz is slightly undersaturated. Finally, after the destruction of magnetite at point C, a weathering assemblage dominated by clays forms, similar to that of the leached zone. Unlike the leached zone, however, pyrite and bornite are also stable phases.

In the protore zone, various combinations of the protore minerals are stable during the simulation. The results of weathering produce relatively little change and are manifested by the formation of Na nontronite ($Na_{0.33}Fe_2Al_{10.33}Si_{3.67}O_{10}(OH)_2$) during steady state 1, Ca nontronite during steady states 2, 3, and 4, and epidote throughout the simulation. The formation of small amounts of clay is consistent with petrographic observations (cf. Cunningham, 1984). Although epidote-group minerals may occur replacing feldspars in the pre-Main Stage protore at Butte, it is unclear whether or not any of them formed due to weathering processes. However, the total amount of epidote produced after 12,000 model years is relatively small (about 3.5 vol % in volume element 5). One aspect of the simulation which is not realistic is the complete destruction of magnetite in the protore zone. Magnetite is never close to saturation anywhere in the protore over the course of the simulation, and therefore, the preservation of magnetite in natural systems is probably due to sluggish reaction kinetics. However, the stability of the protore reactants pyrite, chalcopyrite, albite, K-feldspar, muscovite, and quartz at the end of the simulation indicates that, overall, there is a close approach to thermodynamic equilibrium between the aqueous phase and the reactants in the pre-Main Stage protore zone.

The dissolution and precipitation of minerals in the various weathering zones may change porosity within the metasomatic system. Changes in porosity may in turn affect permeability. Although we have neglected this important feedback in the present first-order modeling effort, it is nonetheless useful to examine changes in porosity due to mineral precipitation or dissolution during the simulation. Percent changes in porosity ((porosity at time t − initial porosity) × 100/initial porosity) for the weathering zones are shown in Figure 6A.

In the leached zone, the acid weathering conditions of steady state 1 result in a net increase in porosity due to mineral dissolution. Little volume change occurs after point A, however. In the enrichment blanket, solid volume is added during steady states 1 and 2 causing porosity to decrease. Most of this porosity decrease is due to the precipitation of alunite which has a very high partial molar volume of 293.6 cm^3/mole. During steady states 3 and 4, when pyrite is no longer dissolving in the leached zone and alunite does not form in the blanket zone, the porosity in the en-

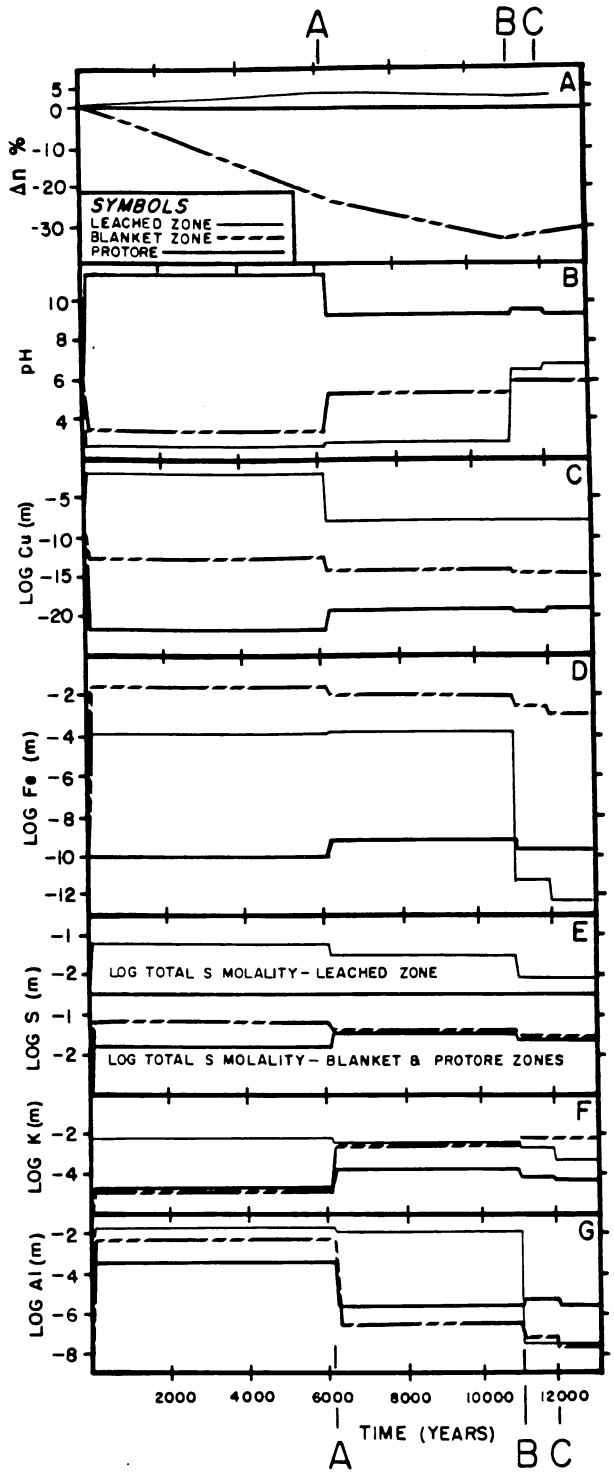

FIG. 6. Porosity changes, pH, and total concentrations (molal) of chemical elements in supergene fluids shown as a function of time. A. percent change in porosity in the leached, blanket, and protore zones. $\Delta n\%$ = (porosity at time t − initial porosity) × 100/initial porosity. B. pH. C. Log total aqueous Cu concentration. D. Log total aqueous Fe concentration. E. Log total aqueous S concentration. F. Log total aqueous K concentration. G. Log total aqueous Al concentration.

richment blanket decreases. Thus the maximum porosity in the enrichment blanket is attained immediately before the destruction of all primary sulfides in the leached zone. The protore is little modified during the course of weathering and hence its porosity stays approximately constant throughout the simulation.

Chemical element mobility

Numerical modeling provides a means with which to assess element mobility within the supergene enrichment environment. Following Brimhall and Dietrich (1987) we may divide the behavior of chemical elements into three broad categories. Residual elements are completely immobile and are not transported by meteoric waters. Supergene elements are leached from a source region and then reprecipitated in an enrichment zone farther along the flow path within the weathering system. Mobile elements are leached during weathering but are not reprecipitated within the metasomatic system of interest and leave in discharging fluids. In addition, the behavior of a given element may change with time in response to variations in the geochemical environment caused by events such as the complete dissolution of a mineral phase within some portion of the flow region.

Before investigating the mobility of chemical elements within the weathering system, we examine the pH of the metasomatic fluids through time owing to the importance of hydrogen ion activity in controlling mineral solubilities. Figure 6B shows variations in pH with time for the leached, blanket, and protore zones. It should be noted that the changes which occur in solution composition at points A, B, and C appear to be very abrupt because in this particular simulation it takes a relatively short time, on the order of 140 yr, to attain steady state behavior throughout the flow region after the complete dissolution of a protore reactant occurs.

Owing to the dissolution of primary chalcopyrite and pyrite by oxygenated fluids, the pH values of the leached zone remain low, between 2.7 and 2.8, until point B when all sulfides have been destroyed in the leached zone. The following overall reactions illustrate the generation of acid fluids and formation of hematite during sulfide dissolution:

$$15/2O_2 + 4H_2O + 2FeS_2 \rightarrow Fe_2O_3 + 4SO_4^{-2} + 8H^+ \quad (8)$$

and

$$17/2O_2 + 2H_2O + 2CuFeS_2 \rightarrow 2Cu^{+2} + Fe_2O_3 + 4SO_4^{-2} + 4H^+. \quad (9)$$

These reactions show that the conversion of pyrite to hematite produces more hydrogen ions than the conversion of chalcopyrite to hematite. Also, in the pre-Main Stage protore simulation, pyrite has twice the reactive surface area of chalcopyrite. Therefore in this protore, it is hematite precipitation caused by pyrite dissolution that generates most of the hydrogen ions, which accounts for the relatively small change in pH after chalcopyrite is destroyed in the leached and blanket zones at point A. After pyrite is dissolved completely from the leached zone, solution pH rapidly shifts to values in the neutral range.

In the blanket zone, pH remains low during the formation of the enrichment blanket owing to operation of precipitation reactions of the form:

$$2H_2O + 3Cu^{+2} + CuFeS_2 \rightarrow 2Cu_2S + Fe^{+2} + 4H^+ + O_2. \quad (10)$$

After chalcopyrite is destroyed in both the leached and blanket zones (point A) and enrichment blanket formation stops, pH moves to higher values between 5 and 6.

The pH of the protore zone is always alkaline. The highest pH values occur when the copper enrichment blanket is forming during steady state 1. After point A, solution pH stays within the range of 9 to 9.5. Solution pH values in the range of 9 to 9.5 have been measured in the unoxidized portions of sulfide orebodies by Baas Becking et al. (1960) and Sato (1960). The simulation results therefore are in good agreement with pH measurements in natural systems. Protore zone fluids do not become acidic because primary Cu-Fe sulfides are stable there.

Unsurprisingly, Cu displays the most pronounced supergene behavior in the weathering system (Fig. 6C). During steady state 1 as chalcopyrite dissolves (see eq. 9), the total copper concentration of approximately 10^{-2} molal in the leached zone is quite high. After point A, chalcopyrite no longer dissolves and the copper content of the fluids in the leached zone is the same as that of the incoming rainwater. The copper molality in the blanket zone is always between 10^{-15} and 10^{-13} molal, indicating nearly complete fixation of Cu in the enrichment blanket. The aqueous copper concentration in the protore is even lower and ranges from 10^{-22} to 10^{-20} molal.

Iron displays essentially immobile behavior (Fig. 6D). During acid weathering conditions in the leached zone over steady states 1 and 2, Fe concentrations are moderate and remain close to 10^{-4} molal. Most of the iron liberated by sulfide dissolution is fixed in hematite, however (see eq. 8 and 9). After point B is reached, Fe concentrations in the leached zone drop drastically to levels between about 10^{-11} and 10^{-12} molal, indicating that very little Fe transport out of the leached zone takes place after primary sulfides have been destroyed and pH values increase. The Fe content of fluids in the copper enrichment blanket remains high, between 10^{-3} and 10^{-2} molal, throughout the simulation whereas that of the protore zone

is considerably lower, ranging between 10^{-10} and 10^{-9} molal.

Unlike Cu, S displays a high degree of mobility (Fig. 6E). Throughout the simulation, the S contents of fluids in all zones of the weathering system are quite high and are always between 10^{-2} and 10^{-1} molal. Thus a substantial amount of S, primarily in the form of SO_4^{-2}, leaves the flow region through time. K concentrations are in the range between 10^{-5} and 10^{-2} molal during the simulation (Fig. 6F). The concentration of K in fluids leaving the base of the system considered here varies between about 10^{-5} and 10^{-4} molal, indicating a moderate degree of K mobility.

Al displays the most complex behavior of any chemical element considered in this study (Fig. 6G). During steady state 1, the Al molalities in all zones are relatively high. The leached zone fluids have the highest concentrations of Al, approximately 2×10^{-2} molal, whereas the blanket and protore zone fluid molalities of 4×10^{-3} and 3×10^{-4} molal, respectively, are lower. The mobility of Al during steady state 1 may be explained by the low pH values in the leached zone and blanket zone and the high pH in the protore zone because Al may be transported in solution at both low and high pH. However, after point A is reached the pH in the blanket zone increases whereas the pH in the protore zone decreases. Therefore, Al contents in the blanket and protore zones decrease from the levels attained during steady state 1 to about 3×10^{-7} and 3×10^{-6} molal, respectively. Owing to low pH, the Al concentration in the leached zone remains quite high at approximately 10^{-2} molal. Thus under steady state 2, Al behaves approximately as a supergene element because it is transported out of the leached zone and fixed to a high degree in solid phases, predominantly clays, below the ground-water table. After pyrite dissolves from the leached zone at point B, the Al content of fluids throughout the weathering system are low, due to clay precipitation, and range from 10^{-5} to 10^{-8} molal. Here, nearly residual behavior is displayed because very little Al is transported between any of the weathering zones or out of the flow region.

The elements Si, Ca, and Na, not shown in Figure 6, are mobile to varying degrees. The concentration of Si in all weathering zones is always close to 10^{-4} molal indicating a moderate degree of mobility. The Ca and Na contents of the fluids are even higher, generally between 10^{-3} and 10^{-2} molal, and therefore a substantial amount of these elements are transported out of the weathering system with time.

The almost complete fixation of Cu in the blanket zone by precipitation of secondary sulfides strongly supports the assumptions made by Brimhall et al. (1985) that vertical Cu fluxes out of an enrichment system are insignificant even over long periods of geologic time. For example, using the flow rate of this study (0.2 m^3/yr) and the average Cu concentration of the blanket zone fluids of 10^{-14} molal, it would take on the order of 10^{12} yr for one mole of Cu to be transported out of the blanket zone. However, lateral fluid fluxes in the unsaturated zone may, during leaching, transport significant Cu away from the region of chalcopyrite dissolution (cf. Newberg, 1967; Mortimer et al., 1977). It is almost certain, therefore, that the inefficiency in Cu fixation observed in some natural deposits (cf. Brimhall et al., 1985) is due to lateral copper fluxes because any copper which descends along a vertical flow path beneath the ground-water table is quantitatively fixed in the blanket zone. Thus, reconstructions of paleotopography and determinations of amounts of erosion and erosion rates in regions of vertical fluid flow using copper mass balances (cf. Brimhall et al., 1985; Brimhall and Dietrich, 1987; Alpers and Brimhall, 1988, 1989) should be sufficiently accurate.

Al exhibits mobile, supergene, and residual behavior under different conditions at different times during the simulation. This suggests that abundance patterns of Al in vertical weathering profiles and paleosols should be interpreted with considerable caution.

In sharp contrast to the supergene element copper, sulfur, dominantly in the form of SO_4^{-2}, is the most mobile element in the weathering system. This is realistic because the rates of inorganic sulfate reduction at low temperatures are extremely slow (Ohmoto and Lasaga, 1982). The dominant source of sulfur for the precipitation of secondary sulfides in the blanket zone in the modeling was the preexisting protore sulfides (see eq. 10), not the sulfate transported from the leached zone. This is in accord with the common replacement textures observed in supergene ores and the very slow rates of inorganic sulfate reduction in weathering environments.

The elements Si, K, Na, and Ca are generally mobile in the weathering system. The concentration of $SiO_{2(aq)}$ in the fluids varies little and is always close to 10^{-4} molal because quartz is typically saturated or nearly so in this weathering environment. The alkali metals K, Na, and Ca are liberated into the fluids by feldspar and mica hydrolysis. Significant quantities of these elements may be removed from the flow region, as has been observed in numerous natural weathering systems (cf. Brimhall and Dietrich, 1987).

Mineral stability relationships and the chemical evolution of supergene fluids

We now discuss mineral stability relationships in terms of activities of ions in solution, gas fugacities, and the Eh-pH characteristics of the weathering fluids. Using appropriate phase diagrams, we may examine solution compositions and stable mineral assemblages during steady-state behavior and also the geochemical

response of the weathering environment to the complete dissolution of protore reactants within the flow region.

Activities of H^+, K^+, and SO_4^{-2} in solution: The phases alunite, kaolinite, muscovite (sericite), and K-feldspar may be stable at various times and locations within the weathering profile. Depiction of both the evolution of fluid compositions and the stability relations of these minerals on a single diagram, using the negative logarithms of $a_{K^+}^2 a_{SO_4^{-2}}$ and $a_{H^+}^2 a_{SO_4^{-2}}$ as axes (Hemley et al., 1969), illustrates major differences in the reaction paths of the leached, blanket, and protore zones (Fig. 7).

In the leached zone (Fig. 7A), oxidative weathering and dissolution of primary sulfides by overall reactions of the form of equations (8) and (9) generates H^+ and SO_4^{-2} which causes the solution composition to move from the starting rainwater composition, in the kaolinite stability field, into the alunite field where it remains for both steady states 1 and 2. Note that the disappearance of chalcopyrite in the leached zone, which causes the aqueous phase composition to move from steady state 1 to steady state 2 (Fig. 7A), has a relatively minor effect on the activities of H^+, K^+, and SO_4^{-2} in solution. After pyrite is destroyed in the leached zone signaling the end of steady state 2, the solution composition shifts back to significantly lower activities of H^+ such that muscovite (sericite) is stable during steady state 3 (Fig. 7A). After magnetite is destroyed in the system the solution composition moves into equilibrium with both kaolinite and muscovite (sericite) during steady state 4.

In the blanket zone, fluids are initially highly alkaline and sulfate poor with $-\log (a_{H^+}^2 a_{SO_4^{-2}})$ values as high as 32 (Fig. 7B) illustrating the control of the minerals in the protore in buffering solution composition. However, after 12 yr of simulation time, appreciable quantities of acid sulfate- and copper-rich fluids arrive from the overlying leached zone causing $a_{K^+}^2 a_{SO_4^{-2}}$ and $a_{H^+}^2 a_{SO_4^{-2}}$ to increase by approximately 10 and 20 orders of magnitude, respectively. The solution composition enters the alunite stability field where it remains for steady states 1 and 2. After pyrite dissolves from the leached zone, the activities of H^+, K^+, and SO_4^{-2} decrease such that kaolinite and muscovite (sericite) are stable during steady states 3 and 4.

In strong contrast to the leached zone and enrichment blanket, fluids in the protore remain alkaline throughout the simulation at values of $a_{H^+}^2 a_{SO_4^{-2}}$ as much as 20 orders of magnitude less than those attained in the overlying zones (Fig. 7C). This illustrates the buffering of the fluid composition by the minerals in the pre-Main Stage protore which is out of contact with oxygenated meteoric waters. The protore phases K-feldspar and muscovite are stable throughout much of the simulation and, during steady state 4, the final

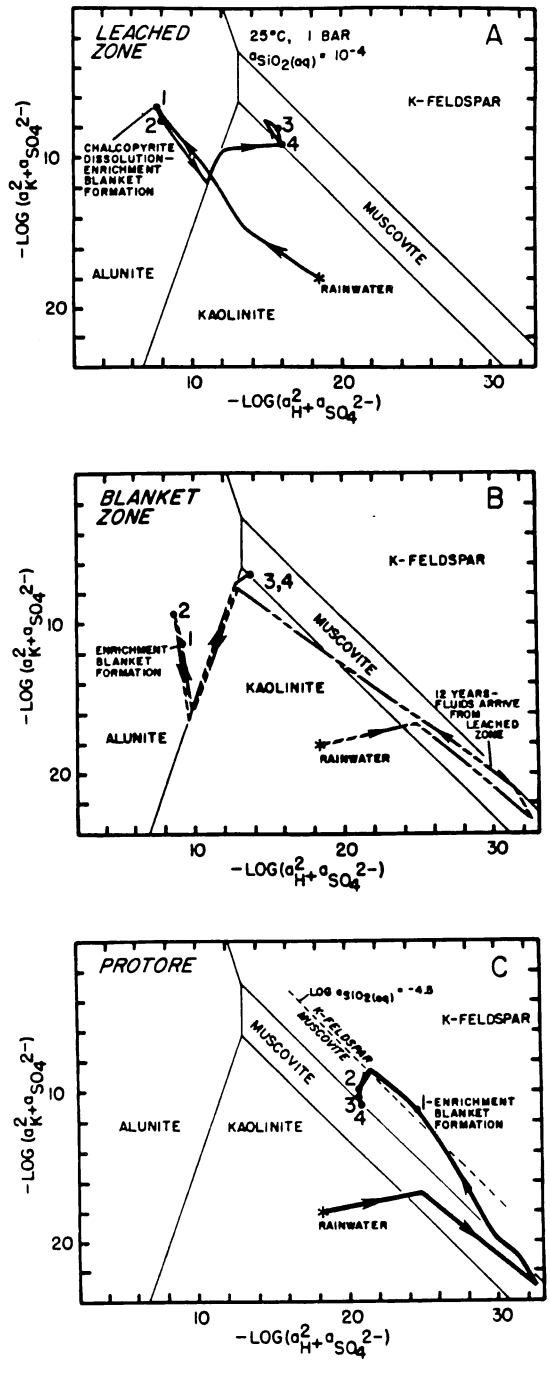

FIG. 7. $-\text{Log}\ (a_{K^+}^2 a_{SO_4^{-2}})$ versus $-\log (a_{H^+}^2 a_{SO_4^{-2}})$ (cf. Hemley et al., 1969). Numbers represent solution composition during steady states 1 (140–6,170 years), 2 (6,310–11,030 years), 3 (11,180–11,870 years), and 4 (>12,010 years). Because quartz is at or near saturation in the flow region throughout the simulation, equilibrium phase boundaries are drawn for the quartz-saturated case ($a_{SiO_2(aq)} = 10^{-4}$). A. Leached zone. B. Enrichment blanket. Note increase in activities of H^+, K^+, and SO_4^{-2} as fluids arrive from the leached zone after 12 years of model time. C. Protore. Note that K-feldspar and muscovite are stable during steady states 2, 3, and 4 but during steady states 2 and 3 quartz is slightly undersaturated.

assemblage of K-feldspar, muscovite, and quartz depicted in Figure 7C indicates a close approach to equilibrium between aqueous solution and protore.

Oxygen and sulfur fugacities: Sulfur-oxygen fugacity diagrams may be used to show the stability relations of the sulfides and oxides within the weathering environment (Holland, 1959, 1965) and also important silicate and sulfate phases such as K-feldspar, annite, muscovite, and alunite (Brimhall, 1980). Sulfur-oxygen fugacity diagrams for the blanket and protore zones are shown in Figure 8A and B. The leached zone plots well off these diagrams at oxygen fugacities of 10^{-35} and extremely low f_{S_2} values of approximately 10^{-100}.

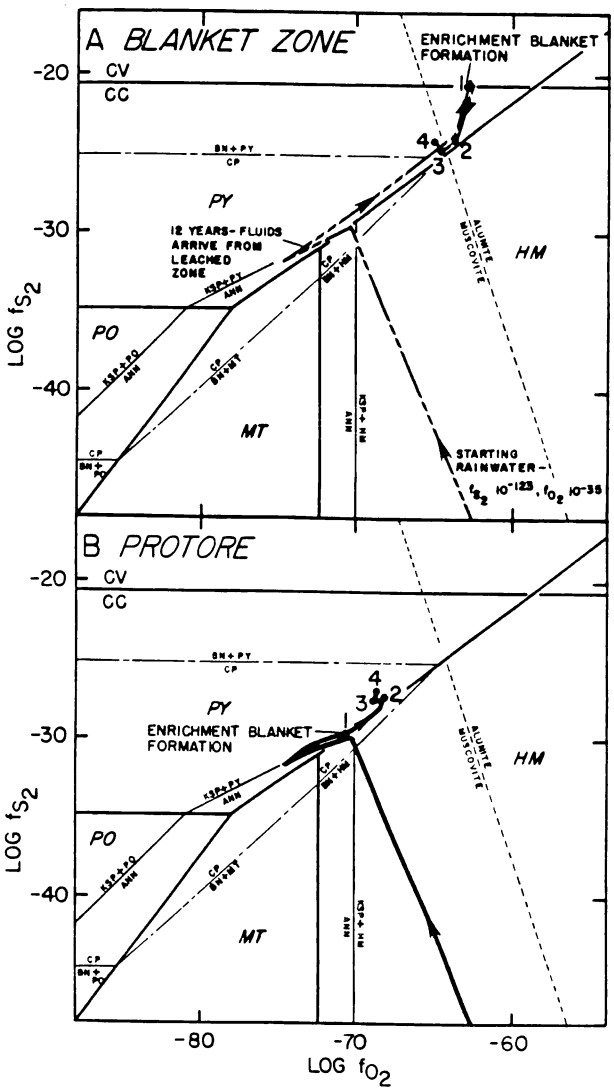

FIG. 8. Log f_{S_2} versus log f_{O_2}. A. Enrichment blanket. B. Protore. Leached zone plots off these diagrams at $f_{S_2} = 10^{-100}$ and $f_{O_2} = 10^{-35}$. Abbreviations: ANN = annite, BN = bornite, CC = chalcocite, CP = chalcopyrite, CV = covellite, HM = hematite, KSP = K-feldspar, MT = magnetite, PO = pyrrhotite, PY = pyrite.

In the enrichment blanket, the starting rainwater initially comes into equilibrium with the protore minerals K-feldspar, annite, pyrite, and chalcopyrite (Fig. 8A). However, after 12 years of model time, the influx of oxygenated copper- and sulfate-rich fluids from the leached zone causes increases in both f_{O_2} and f_{S_2} of approximately 10 orders of magnitude such that the chalcocite, covellite, and pyrite of the enrichment blanket are stable during steady state 1. After chalcopyrite dissolves completely from the leached and blanket zones, f_{S_2} and f_{O_2} decrease by about 4 and 1 orders of magnitude, respectively. Pyrite and bornite are then the stable sulfide phases for the rest of the simulation. This suggests that in the weathering and supergene enrichment of protore similar to the pre-Main Stage at Butte, bornite, if it occurs as a supergene mineral, may postdate chalcocite and covellite in the enrichment blanket. Also, preservation of the blanket would require that the transformation of chalcocite and covellite to bornite be very slow. However, in natural systems, primary chalcopyrite and pyrite may never be completely destroyed in the leached zone which would tend to keep f_{S_2} elevated in the enrichment blanket such that chalcocite and covellite could be stable. A further consideration is that supergene idaite (Cu_5FeS_6) may form in lieu of bornite because the two phases are structurally and compositionally similar. For example, at the Ok Tedi deposit, idaite is common in the enrichment blanket but rare in the underlying protore (K. Danti, pers. commun., 1987) suggesting that idaite may have formed as a result of weathering.

During steady state 1 the protore remains in equilibrium with annite, pyrite, and chalcopyrite (Fig. 8B). After chalcopyrite dissolves in the leached zone and enrichment blanket, f_{S_2} and f_{O_2} increase slightly. For the remainder of the simulation, Figure 8B shows that K-feldspar, pyrite, and chalcopyrite are stable. The changes in f_{S_2} and f_{O_2} in the protore over the course of the simulation are much smaller than those which occur in the enrichment blanket owing to the buffering potential of the protore minerals in the absence of oxygenated meteoric fluids.

Fe^{+2}-Cu^{+}-H_2S diagrams: Triple point diagrams (Brimhall, 1980) allow the depiction of sulfide and oxide stability relations in terms of the aqueous base metal activity ratio $a_{Fe^{+2}}/a^2_{Cu^+}$ as a function of $f_{H_2S_{(g)}}$ without having to specify activities of other ions in solution such as H^+ (Fig. 9). The leached zone plots off of the diagrams of Figure 9 at log $(a_{Fe^{+2}}/a^2_{Cu^+})$ in the range of 6 to 13 and log $f_{H_2S_{(g)}}$ values of approximately −70.

In the blanket zone (Fig. 9A), prior to the introduction of fluid from the leached zone, log $(a_{Fe^{+2}}/a^2_{Cu^+})$ is high at 33. Once blanket formation begins after 12 years of simulation, there is a 10 order of magnitude drop in $a_{Fe^{+2}}/a^2_{Cu^+}$ as the fluid comes to

equilibrium with pyrite, covellite, and chalcocite (Fig. 9A). At the end of steady state 1 when chalcopyrite is dissolved from the leached zone and blanket zone, $f_{H_2S_{(g)}}$ decreases by about 1.5 orders of magnitude whereas $a_{Fe^{+2}}/a^2_{Cu^+}$ increases by approximately 4 orders of magnitude such that pyrite and bornite are the stable sulfides in steady states 2, 3, and 4. In the protore, $a_{Fe^{+2}}/a^2_{Cu^+}$ remains at least 2 orders of magnitude higher than in the blanket zone during steady states 1, 2, 3, and 4 causing pyrite and chalcopyrite to be the stable sulfide minerals.

Eh-pH conditions: Eh-pH diagrams (cf. Baas Becking et al., 1960; Garrels and Christ, 1965) permit evaluation of the general oxidizing or reducing nature of the various weathering zones and also the stability relations of mineral phases and aqueous species as a function of hydrogen ion activity (Fig. 10).

The solution compositions in the leached zone fall within the empirically defined field for natural aerated meteoric waters (Fig. 10A; Garrels and Christ, 1965). Dissolution of sulfides causes pH to drop and Eh to increase, under the condition that f_{O_2} is buffered at 10^{-35}, so that during steady state 1 Cu^{+2} is an important component of the aqueous phase and hematite (and/or goethite) precipitates (see eq. 8 and 9). After pyrite dissolves completely from the leached zone, solution pH increases and Eh decreases so that the Eh-pH conditions of fluids in the unsaturated zone are very similar to the incoming rainwater during steady states 3 and 4.

The fluids in the blanket zone display radically different behavior (Fig. 10A). As discussed above, initial equilibration of protore with the starting rainwater causes pH to increase. At the same time, oxidation potential greatly decreases to values appropriate for ground waters (cf. Garrels and Christ, 1965). After 12 years of simulation, acid fluids begin arriving from the leached zone and pH decreases in the enrichment

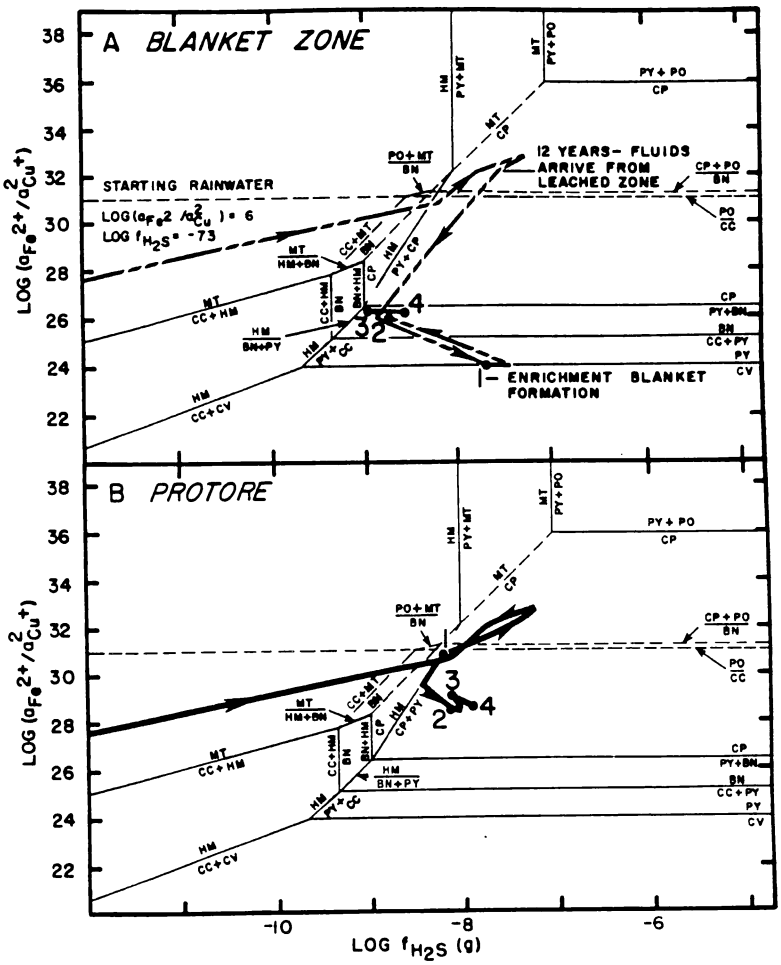

FIG. 9. Log $a_{Fe^{+2}}/a^2_{Cu^+}$ versus log $f_{H_2S_{(g)}}$ (Brimhall, 1980). A. Enrichment blanket. B. Protore. Leached zone plots off these diagrams at log ($a_{Fe^{+2}}/a^2_{Cu^+}$) = 6–13 and log $f_{H_2S_{(g)}}$ = −70. See Figure 8 for abbreviations.

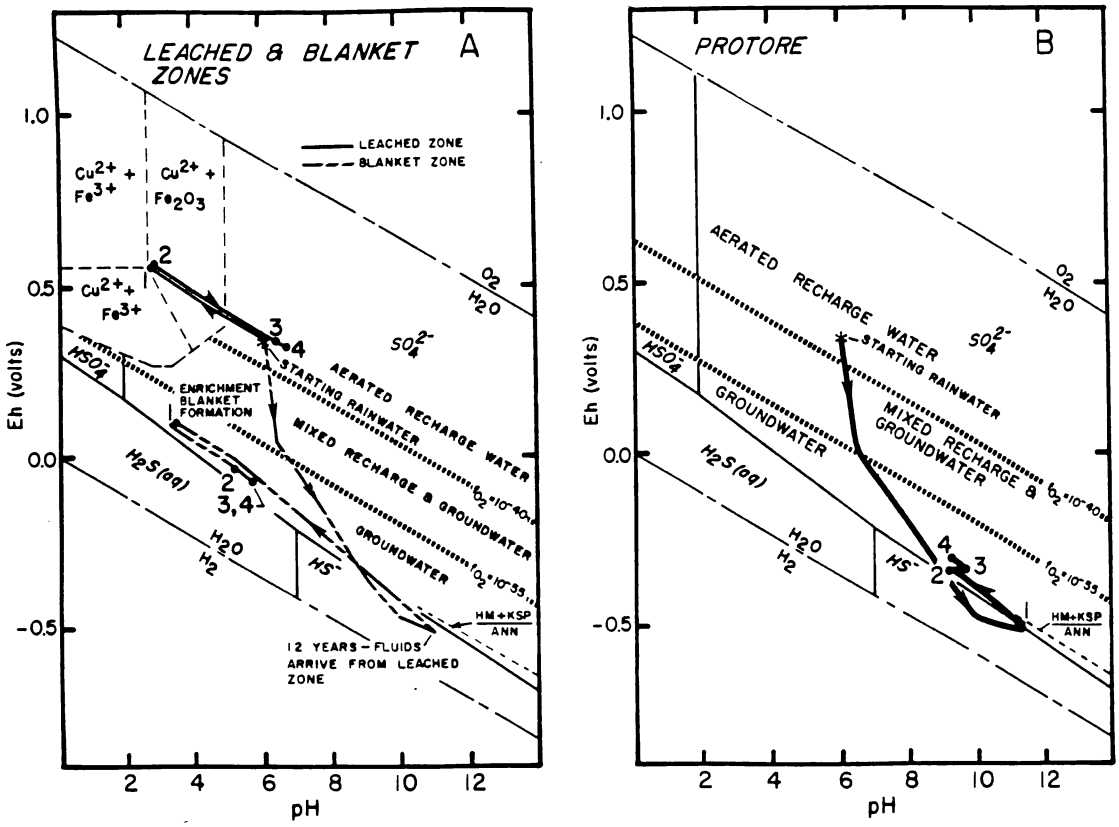

FIG. 10. Eh versus pH. A. Leached zone and enrichment blanket. The average activities of Fe^{+2}, Fe^{+3}, and Cu^{+2} during steady state 1 were used to draw equilibrium boundaries involving Fe^{+2}, Fe^{+3}, Cu^{+2}, and hematite. Values used: $\log a_{Fe^{+2}} = -4.4$, $\log a_{Fe^{+3}} = -8.0$, $\log a_{Cu^{+2}} = -2.3$. B. Protore. Fields for aerated waters, mixed waters, and ground waters from Garrels and Christ (1965). See Figure 8 for abbreviations.

blanket to about 3.5 as secondary sulfides precipitate liberating H^+ (see eq. 10). After chalcopyrite dissolves completely from the leached and blanket zones and chalcocite and covellite no longer precipitate in the blanket, pH values move to less acid values between 5 and 6 during steady states 2, 3, and 4. The protore fluids are alkaline throughout the simulation and oxidation potentials are very low (Fig. 10B). The protore stays at or close to equilibrium with K-feldspar, annite, and hematite (Fig. 10B). The oxidation potential of the protore is lower than that of the enrichment blanket because of the constant influx of oxygenated meteoric waters into the blanket zone from the leached zone. Figure 10A and B show that during steady states 1, 2, 3, and 4 SO_4^{-2} is the dominant sulfur species in all the weathering zones.

In summary, it is clear from the diagrams presented above that the geochemical evolutions of fluids within the leached, blanket, and protore zones are dramatically different. The fundamental control on the nature and degree of chemical reequilibration which takes place is the oxygen fugacity within a given weathering zone. Thus the rocks in the unsaturated zone, which are in intimate contact with the atmosphere and oxygenated meteoric waters, undergo extensive chemical modification by highly acid copper- and sulfate-rich ore-forming fluids generated by the dissolution of pyrite and chalcopyrite in this oxidative environment. At the other extreme is the stable protore which is out of direct contact with the atmosphere. Here, pH values are alkaline and the oxidation potential of fluids is low due to buffering by mineral assemblages in the rock. Therefore, little chemical modification of the protore takes place with time. Broadly speaking, the blanket zone may be described as the interface between these highly oxidizing and highly reducing extremes of the atmosphere and the continental hydrosphere. The approximately 30 orders of magnitude decrease in oxygen fugacity attending the transition from water-unsaturated to water-saturated conditions causes oxygenated ore-forming fluids entering the enrichment blanket from the leached zone to precipitate secondary copper sulfides. The differentiated hydrochemical system represents a closer approach to overall equilibrium under steady-state flow conditions.

The destruction of primary sulfide minerals within the leached and blanket zones causes considerable changes in fluid composition and precipitated mineral assemblages. For example, although acid weathering conditions continue in the leached zone after chalcopyrite dissolves, the blanket zone fluids undergo a significant increase in pH and decrease in Eh because secondary sulfides are no longer precipitating in the enrichment blanket. When pyrite dissolves from volume elements 1 and 2, leached zone fluids rapidly move to pH values in the neutral range. Relatively little change in fluid compositions or stable mineral assemblages occurs when magnetite is dissolved from the weathering system. At the end of the simulation, the stable mineral assemblages in the leached and blanket zones are dominated by silicate clays. However, in the enrichment blanket, pyrite and bornite are also stable, owing to low oxygen fugacities, whereas all sulfides have been destroyed in the oxidative conditions of the overlying leached zone.

Conclusions

In this study we have developed a numerical model which explicitly couples advective solute transport and chemical reaction in order to investigate weathering and supergene enrichment of porphyry copper deposits. The model is general and may also be applied to other low-temperature weathering and ore-forming metasomatic environments. The supergene system consisting of the leached zone, blanket zone, and protore has been modeled as a single differentiated hydrochemical system in order to gain insights into the complex interrelationships between ore-forming fluid formation, solute transport, and mineral dissolution and precipitation. The mineral assemblages computed by the model agree well with those observed in nature which strongly suggests that the computational procedure developed herein is a valid first approximation for simulation of fluid-rock interactions and solute transport in low-temperature oxidative environments. We have therefore attempted to outline the evolution of supergene systems under steady flow conditions during the ore-forming stage and later, when phases essential to supergene enrichment, such as pyrite and chalcopyrite, dissolve completely from the leached zone. In addition, the modeling provides a way in which to investigate element mobility between the various weathering zones and out of the supergene enrichment system altogether and thus provides constraints on the interpretation of chemical element abundance patterns in natural weathering profiles and paleosols.

Numerical modeling of coupled fluid flow and chemical reaction can provide insights into the long-term evolution of complex metasomatic environments which would be otherwise difficult or impossible to obtain given the short time span of direct observation. The modeling effort also highlights a number of exciting research problems, such as the feedback between chemical reaction and changes in both rock permeability and reactive surface areas of minerals, which require vigorous investigation in order to increase the realism and predictive capabilities of numerical models and ultimately to broaden our understanding of surficial weathering processes and hydrochemical systems in general. While we have focused here on a steady-state flow regime, recent petrologic advances in dynamic supergene systems which evolve under transient ground-water flow conditions (Alpers and Brimhall, 1988, 1989) present great opportunities for simulating the effects of climatic change on supergene hydrochemical processes. Interrelationships between surficial processes are beginning to be understood including climatic change, rates of erosion, and preservation of enriched ore-forming systems.

Acknowledgments

Thoughtful discussions with Daria Ague, Charles Alpers, Kathy Danti, Bill Dietrich, Chris Lewis, Peter Lichtner, T. N. Narasimhan, Tetsu Tokunaga, and Cathy Wilson have contributed greatly to this work. In particular, we thank Aric Cunningham for allowing us to use his unpublished data. The expert advice and technical assistance of John Donovan, Joachim Hampel, Len Vigus, and Tim Teague proved to be invaluable. D. M. Rimstidt and P. M. Gagen generously provided unpublished data on the dissolution rates of sulfides. Tom Wolery and Ken Jackson of Lawrence Livermore National Laboratory deserve special recognition for providing computer programs and excellent technical advice. We would also like to thank the staff at Ok Tedi Mining Pty. Ltd. for their hospitality, logistical support, and scientific insights during field work in Papua New Guinea. National Science Foundation funding (EAR 84-16790) made this study possible and is gratefully acknowledged.

August 8, 1988; January 18, 1989

REFERENCES

Alpers, C. N., and Brimhall, G. H., 1988, Middle Miocene climatic change in the Atacama Desert, northern Chile: Evidence from supergene mineralization at La Escondida: Geol. Soc. America Bull., v. 100, p. 1640–1656.

—— 1989, Paleohydrologic evolution and geochemical dynamics of cumulative supergene metal enrichment at La Escondida, Atacama desert, northern Chile: ECON. GEOL., v. 84, p. 229–254.

Anderson, T. A., 1982, Characteristics of leached capping and techniques of appraisal, *in* Titley, S. R., ed., Advances in the geology of porphyry copper deposits, southwestern North America: Tucson, Univ. Arizona Press, p. 275–295.

Baas Becking, L. G. M., Kaplan, I. R., and Moore, D., 1960, Limits of the natural environment in terms of pH and oxidation-reduction potentials: Jour. Geology, v. 68, p. 243–284.

Bamford, R. W., 1972, The Mount Fubilan (Ok Tedi) porphyry copper deposit, Territory of Papua and New Guinea: ECON. GEOL., v. 67, p. 1019–1033.

Bateman, A. M., 1950, Economic mineral deposits: New York, John Wiley, p. 245–287.

Berner, R. A., 1969, Goethite stability and the origin of red beds: Geochim. et Cosmochim. Acta, v. 33, p. 267–273.

—— 1971, Principles of chemical sedimentology: New York, McGraw-Hill, 240 p.

Bladh, K. W., 1982, The formation of goethite, jarosite, and alunite during the weathering of sulfide-bearing felsic rocks: ECON. GEOL., v. 77, p. 176–184.

Blain, C. F., and Andrew, R. L., 1977, Sulfide weathering and the evaluation of gossans in mineral exploration: Minerals Sci. Eng., v. 9, p. 119–149.

Blanchard, R., 1968, Interpretation of leached outcrops: Nevada Bur. Mines Bull., v. 66, 196 p.

Brace, W. F., 1980, Permeability of crystalline and argillaceous rocks: Internat. Jour. Rock Mechanics Mineral Sci. Geomechanics, Abstracts, v. 17, p. 241–251.

Braithwaite, J. W., 1976, Simulated deep solution mining of chalcopyrite and chalcocite: Unpub. Ph.D. thesis, Univ. Utah, 255 p.

Brimhall, G. H, Jr., 1977, Early fracture-controlled disseminated mineralization at Butte, Montana: ECON. GEOL., v. 72, p. 37–59.

—— 1979, Lithologic determination of mass transfer mechanisms of multiple-stage porphyry copper mineralization at Butte, Montana: Vein formation by hypogene leaching and enrichment of potassium silicate protore: ECON. GEOL., v. 74, p. 556–589.

—— 1980, Deep hypogene oxidation of porphyry copper potassium-silicate protore at Butte, Montana: A theoretical evaluation of the copper remobilization hypothesis: ECON. GEOL., v. 75, p. 384–409.

Brimhall, G. H, and Ague, J. J., 1989, Granitic systems, *in* Barnes, H. L., and Ohmoto, H., eds., Hydrothermal processes—applications to ore genesis: Holland, Reidel.

Brimhall, G. H, and Dietrich, W. E., 1987, Constitutive mass balance relations between chemical composition, volume, density, porosity and strain in metasomatic hydrochemical systems: Results on weathering and pedogenesis: Geochim. et Cosmochim. Acta, v. 51, p. 567–587.

Brimhall, G. H, and Ghiorso, M. S., 1983, Origin and ore-forming consequences of the advanced argillic alteration process in hypogene environments by magmatic gas contamination of meteoric fluids: ECON. GEOL., v. 78, p. 73–90.

Brimhall, G. H, Alpers, C. N., and Cunningham, A. B., 1985, Analysis of supergene ore-forming processes and ground-water solute transport using mass balance principles: ECON. GEOL., v. 80, p. 1227–1256.

Busenberg, E., and Clemency, C. V., 1976, The dissolution kinetics of feldspars at 25°C and 1 atm CO_2 partial pressure: Geochim. et Cosmochim. Acta, v. 40, p. 41–49.

Cathles, L. M., 1979, Predictive capabilities of a finite difference model of copper leaching in low grade industrial sulfide waste dumps: Math. Geology, v. 11, p. 175–191.

Cathles, L. M., and Apps, J. A., 1975, A model of the dump leaching process that incorporates oxygen balance, heat balance, and air convection: Metall. Trans., v. 6B, p. 617–624.

Cederberg, G. A., 1985, TRANQL: A groundwater mass transport and equilibrium chemistry model for multicomponent systems: Unpub. Ph.D. thesis, Stanford Univ., 117 p.

Cunningham, A. B., 1984, Geologically constrained hydrologic and geochemical modeling of supergene weathering processes using physical and modal data: Unpub. M.S. thesis, Univ. California, Berkeley, 122 p.

De Donder, T., and Rysselberghe, P. V., 1936, Thermodynamic theory of affinity: A book of principles: Stanford, California, Stanford Univ. Press, 142 p.

Delany, J. M., Puigdomenech, I., and Wolery, T. J., 1986, Precipitation kinetics option for the EQ6 geochemical reaction path code: Lawrence Livermore Natl. Lab. Bull. UCRL-53642, 44 p.

Dutt, G. R., Shaffer, M. J., and Moore, W. J., 1972, Computer model of dynamic biophysicochemical processes in soils: Univ. Arizona Tech. Bull. 196, 101 p.

Elias, M., Donaldson, M. J. M., and Giorgetta, N. E., 1981, Geology, mineralogy and chemistry of lateritic nickel-cobalt deposits near Kalgoorlie, western Australia: ECON. GEOL., v. 76, p. 1775–1783.

Emmons, W. H., 1918, The principles of economic geology: New York, McGraw-Hill, 153 p.

Freeze, R. A., and Cherry, J. A., 1979, Groundwater: Englewood Cliffs, New Jersey, Prentice-Hall, 604 p.

Gagen, P. M., 1987, The oxidation rates of arsenopyrite and chalcopyrite in acidic ferric chloride solutions at 0 to 60°C: Unpub. M.S. thesis, Blacksburg, Virginia Polytech. Inst., 46 p.

Garrels, R. M., and Christ, C. L., 1965, Solutions, minerals and equilibria: New York, Harper Row, 450 p.

Garven, G., and Freeze, R. A., 1984, Theoretical analysis of the role of groundwater flow in the genesis of stratabound ore deposits. 1. Mathematical and numerical model: Am. Jour. Sci., v. 284, p. 1085–1124.

Golightly, J. P., 1981, Nickeliferous laterite deposits: ECON. GEOL. 75TH ANNIV. VOL., p. 710–734.

Graybeal, K. T., 1982, Geology of the El Tiro area, Pima County, Arizona, *in* Titley, S. R., ed., Advances in the geology of porphyry copper deposits, southwestern North America: Tucson, Univ. Arizona Press, p. 487–505.

Grove, D. B., and Wood, W. W., 1979, Prediction and field verification of subsurface water quality and changes during artificial recharge, Lubbock, Texas: Ground Water, v. 17, p. 250–257.

Helgeson, H. C., 1968, Evaluation of irreversible reactions in geochemical processes involving minerals and aqueous solutions—I. Thermodynamic relations: Geochim. et Cosmochim. Acta, v. 32, p. 853–877.

Helgeson, H. C., Brown, T. H., Nigrini, A., and Jones, T. A., 1970, Calculations of mass transfer in geochemical processes involving aqueous solutions: Geochim. et Cosmochim. Acta, v. 34, p. 569–592.

Helgeson, H. C., Murphy, W. M., and Aagard, P., 1984, Thermodynamic and kinetic constraints on reaction rates among minerals and aqueous solutions. II. Rate constants, effective surface area, and the hydrolysis of feldspar: Geochim. et Cosmochim. Acta, v. 48, p. 2405–2432.

Hemley, J. J., Hostetler, P. B., Gude, A. J., and Mountjoy, W. T., 1969, Some stability relations of alunite: ECON. GEOL., v. 64, p. 599–612.

Holdren, G. R., and Berner, R. A., 1979, Mechanism of feldspar weathering. I. Experimental studies: Geochim. et Cosmochim. Acta, v. 43, p. 1161–1171.

Holland, H. D., 1959, Some applications of thermochemical data to problems of ore deposits. I. Stability relations among the oxides, sulfides, sulfates, and carbonates of ore and gangue minerals: ECON. GEOL., v. 54, p. 184–233.

—— 1965, Some applications of thermochemical data to problems of ore deposits. II. Mineral assemblages and the composition of ore-forming fluids: ECON. GEOL., v. 60, p. 1101–1166.

Jennings, A. A., Kirkman, D. J., and Theis, T. L., 1982, Multicomponent equilibrium chemistry in groundwater quality models: Water Resources Research, v. 18, p. 1089–1096.

Krauskopf, K. B., 1979, Introduction to geochemistry: New York, McGraw-Hill, 617 p.

Langmuir, D., 1971, Particle size effect on the reaction goethite = hematite + water: Am. Jour. Sci., v. 271, p. 147–156.

—— 1972, Correction—particle size effect on the reaction goethite = hematite + water: Am. Jour. Sci., v. 272, p. 972.

Lasaga, A. C., 1984, Chemical kinetics of water-rock interactions: Jour. Geophys. Research, v. 89, p. 4009–4025.

Lichtner, P., 1985, Continuum model for simultaneous chemical reactions and mass transport in hydrothermal systems: Geochim. et Cosmochim. Acta, v. 49, p. 779–800.

Locke, A., 1926, Leached outcrops as guides to copper ores: Baltimore, Williams Wilkens Co., 166 p.
Loghry, J. D., 1972, Characteristics of favorable cappings from several southwestern porphyry copper deposits: Unpub. M.S. thesis, Univ. Arizona, 112 p.
Lowell, J. D., and Guilbert, J. M., 1970, Lateral and vertical alteration-mineralization zoning in porphyry ore deposits: ECON. GEOL., v. 65, p. 373–408.
McClave, M., 1973, Control and distribution of supergene enrichment in the Berkeley pit, Butte district, Montana, *in* Miller, R. N., ed., Guidebook for the Butte Field Meeting of Society of Economic Geologists, Butte, Montana, Aug. 18–21, 1973: Butte, Montana, Anaconda Co., p. k1–k4.
McKibben, M. A., and Barnes, H. L., 1986, Oxidation of pyrite in low temperature acidic solutions: Rate laws and surface textures: Geochim. et Cosmochim. Acta, v. 50, p. 1509–1520.
Meyer, C., 1965, An early potassic type of alteration at Butte, Montana: Am. Mineralogist, v. 50, p. 1717–1722.
Meyer, C., Shea, E. P., Goddard, C. C., Jr., and staff, 1968, Ore deposits at Butte, Montana, *in* Ridge, J. D., ed., Ore deposits of the United States 1933–1967 (Graton-Sales vol.): New York, Am. Inst. Mining Metall. Petroleum Engineers, p. 1363–1416.
Miller, C. W., and Benson, L. V., 1983, Simulation of solute transport in a chemically reactive heterogeneous system: Model development and application: Water Resources Research, v. 19, p. 381–391.
Mortimer, C., Munchmeyer, F. C., and Urqueta, D. I., 1977, Emplacement of the Exotica orebody, Chile: Inst. Mining Metallurgy Trans., v. 86, sec. B, p. B121–127.
Murphy, W. M., 1985, Thermodynamic and kinetic constraints on reaction rates among minerals and aqueous solutions: Unpub. Ph.D. thesis, Univ. California, 160 p.
Narasimhan, T. N., and Witherspoon, P. A., 1976, An integrated finite difference method for analyzing fluid flow in porous media: Water Resources Research, v. 12, p. 57–64.
—— 1977, Numerical model for saturated-unsaturated flow in deformable porous media, 1, Theory: Water Resources Research, v. 13, p. 657–666.
—— 1978, Numerical model for saturated-unsaturated flow in deformable porous media, 3, Application: Water Resources Research, v. 14, p. 1017–1034.
Narasimhan, T. N., Witherspoon, P. A., and Edwards, A. L., 1978, Numerical model for saturated-unsaturated flow in deformable porous media, 2, The algorithm: Water Resources Research, v. 16, p. 255–261.
Narasimhan, T. N., Liu, C., and Brimhall, G. H., 1986a, Numerical simulation of supergene enrichment of copper [abs.]: Geol. Soc. America Abstracts with Programs, v. 18, p. 702.
Narasimhan, T. N., White, A. F., and Tokunaga, T., 1986b, Groundwater contamination from an inactive uranium mill tailings pile, 2, Application of a dynamic mixing model: Water Resources Research, v. 22, p. 1820–1834.
Newberg, D. W., 1967, Geochemical implications of chrysocolla-bearing alluvial gravels: ECON. GEOL., v. 62, p. 932–956.
Nordstrom, D. K., 1982, Aqueous pyrite oxidation and consequent formation of secondary iron minerals, *in* Hossaer, L. R., Kittrick, J. A., and Faming, D. F., eds., Acid sulfate weathering: Madison, Wisconsin, Soil Sci. Soc. America, p. 37–56.
Nordstrom, D. K., and Munoz, J. L., 1986, Geochemical thermodynamics: Palo Alto, Blackwell Sci. Pub., 477 p.
Ohmoto, H., and Lasaga, A. L., 1982, Kinetics of reactions between aqueous sulfates and sulfides: Geochim. et Cosmochim. Acta, v. 46, p. 1727–1745.
Peterson, N. P., Gilbert, C. M., and Quick, G. L., 1951, Geology and ore deposits of the Castle Dome area, Gila County, Arizona: U. S. Geol. Survey Bull. 971, 134 p.
Rasmuson, A., Narasimhan, T. N., and Weretnieks, I., 1982, Chemical transport in a fissured rock: Verification of a numerical model: Water Resources Research, v. 18, p. 1479–1492.
Rimstidt, D., and Barnes, H. L., 1980, The kinetics of silica-water reactions: Geochim. et Cosmochim. Acta, v. 43, p. 1161–1171.
Rubin, J., and James, R. V., 1973, Dispersion-affected transport of reacting solutes in saturated porous media: Galerkin method applied to equilibrium-controlled exchange in unidirectional steady water flow: Water Resources Research, v. 9, p. 1332–1356.
Rye, R. O., Bethke, P. M., and Wasserman, M. D., 1988, Diverse origins of alunite and acid-sulfate alteration: Stable isotope systematics [abs.]: Geol. Soc. America Abstracts with Programs, v. 20, p. A333.
Sato, M., 1960, Oxidation of sulfide ore bodies, 1. Geochemical environments in terms of Eh and pH: ECON. GEOL., v. 55, p. 928–961.
Schulz, H. D., and Reardon, E. J., 1983, A combined mixing cell/analytical model to describe two-dimensional reactive chemical transport for unidirectional groundwater flow: Water Resource Research, v. 19, p. 493–502.
Schwertmann, U., 1985, The effect of pedogenic environments on iron oxide minerals, *in* Stewart, B. A., ed., Advances in soil science: New York, Springer-Verlag, v. 1, p. 171–200.
Tardy, Y., and Nahon, D., 1985, Geochemistry of laterites, stability of Al-goethite, Al-hematite, and Fe^{3+} kaolinite in bauxites and ferricretes: An approach to the mechanism of concretion formation: Am. Jour. Sci., v. 285, p. 865–903.
Titley, S. R., 1978, Geologic history, hypogene features, and processes of secondary sulfide enrichment at the Pleysumi copper prospect, New Britain, Papua New Guinea: ECON. GEOL., v. 73, p. 768–784.
Titley, S. R., and Beane, R. E., 1981, Porphyry copper deposits: ECON. GEOL. 75TH ANNIV. VOL., p. 214–269.
Torrent, J., and Guzman, R., 1982, Crystallization of Fe (III)-oxides from ferrihydrite in salt solutions: Osmotic and specific ion effects: Clay Minerals, v. 17, p. 463–469.
Troeh, F. R., Jabro, J. D., and Kirkham, D., 1982, Gaseous diffusion equations for porous materials: Geoderma, v. 27, p. 239–253.
Wierenga, P. J., Shaffer, M. J., Gomez, S. P., and O'Connor, G. A., 1975, Predicting ionic distributions in large soil columns: Soil Sci. Soc. America Jour., v. 39, p. 1080–1084.
Wiersma, C. L., and Rimstidt, J. D., 1984, Rates of reaction of pyrite and marcasite with ferric iron at pH 2: Geochim. et Cosmochim. Acta, v. 48, p. 85–92.
Wolery, T. J., 1979, Calculation of chemical equilibrium between aqueous solution and minerals: The EQ3/6 softwares package: Univ. California Lawrence Livermore Lab. Bull. UCRL-52658, 31 p.
—— 1983, EQ3NR a computer program for geochemical aqueous speciation-solubility calculations: User's guide and documentation: Univ. California Lawrence Livermore Lab. Bull. UCRL-53414, 191 p.
Wood, B. J., and Walther, J. V., 1983, Rates of hydrothermal reactions: Science, v. 222, p. 413–414.

APPENDIX

Theoretical Approach and Program Execution

Governing equation

The governing equation describing advective transport of chemical species i and changes in the mass of i due to chemical reactions for an arbitrary subvolume l of the flow domain bounded by an enclosing surface Γ_l may be represented as:

$$\underset{\text{(a)}}{\int_{\Gamma_l} K\nabla(z+\psi)\cdot n\, d\Gamma \bar{c}_{i,d\Gamma}} + \underset{\text{(b)}}{M_i \sum_{r=1}^{\hat{r}} \nu_{i,r} R_{r,l}} = \underset{\text{(c)}}{V_{w,l} \frac{\partial c_{i,l}}{\partial t}} \tag{A1}$$

where $c_{i,l}$ = average concentration of species i in an element l [M/L^3], $\bar{c}_{i,d\Gamma}$ = average concentration of species i at the surface segment $d\Gamma$ [M/L^3], K = hydraulic conductivity of the porous medium [L/t], M_i = molecular weight of the ith species [M/mole], r = index number of a chemical reaction, $\hat{r}$ = total number of chemical reactions occurring within element l, $R_{r,l}$ = rate of reaction r in element l [moles/t], t = time, $V_{w,l}$ = volume of water contained in element l [L^3], z = elevation [L], $d\Gamma$ = segment of the bounding surface Γ_l [L^2], Γ_l = closed surface bounding element l [L^2], ψ = piezometric head [L], $\nu_{i,r}$ = stoichiometric coefficient of the ith species in reaction r, positive for products, negative for reactants, and n = unit outer normal to the surface segment $d\Gamma$.

This equation is a formal statement of mass conservation of species i in an aqueous phase. Term (a) describes changes in the mass of i with time within volume element l due to advective fluxes across all bounding surfaces $d\Gamma_l$. Fluid motion is governed by Darcy's law where the Darcy velocity q is given by:

$$q = -K\nabla(z+\psi). \tag{A2}$$

Here, the hydraulic conductivity K is a scalar quantity because in the present study we model the flow region as an isotropic porous medium. Term (b) is a chemical reaction term which represents all changes in the mass of species i with time due to dissolution or precipitation of mineral phases. The summation is over all chemical reactions r occurring within the element l. Term (c) represents the total change in the mass of the ith species in element l with time. We now examine terms (a) and (b) in equation (A1) in detail.

Advective solute transport

Program TRUST solves for fluid flow using an Integral Finite Difference Method (IDFM; Narasimhan and Witherspoon, 1976; Narasimhan et al., 1978). In the IFDM computational scheme, the average physical properties of any volume element l within the flow domain are represented at a point in space contained within l, referred to as a nodal point (Fig. 2). In term (a) of equation (A1), the dot product of $K\nabla(z+\psi)$ with n, the unit outer normal to a given surface segment $d\Gamma$, yields the average Darcy velocity in a direction perpendicular to $d\Gamma$. The product of $K\nabla(z+\psi)\cdot n$ with $d\Gamma\bar{c}_{i,d\Gamma}$ gives the mass of species i traversing the surface segment $d\Gamma$ with time. Using the unit outer normal convention, this product is positive for advective fluxes entering l and negative for fluxes leaving it. Integration over the entire bounding surface Γ therefore gives the total change in the mass of i with time in volume element l due to advection.

Discretization of term (a) in equation (A1) assuming that element l is bounded by stream lines and isopotential lines yields (Narasimhan et al., 1986b):

$$\sum_m F_{lm}\bar{c}_{i,lm} + \sum_b F_{lb}\bar{c}_{i,l} + M_i \sum_{r=1}^{\hat{r}} \nu_{i,r} R_{r,l} = V_{w,l} \frac{\Delta c_{i,l}}{\Delta t} \tag{A3}$$

where b = surface segment which lies on the external boundary of the flow region; the summation over all b represents imposed boundary conditions, m = surface which is completely interior to the flow region, F_{lb} = volumetric water flux into l across an external surface $\Delta\Gamma_{lb}$ [L^3/t], and F_{lm} = volumetric water flux into l across an internal surface $\Delta\Gamma_{lm}$ [L^3/t]. TRUST computes the summations of all advective fluxes F_{lm} and F_{lb} for all volume elements in the flow region.

We have modeled the advective mixing of solute species as a titration process in which the composition of the advectively mixed fluid within any volume element l is assumed to be homogeneous at all times. Although molecular diffusion and mechanical dispersion will act to homogenize the composition of fluid within l, we have neglected these effects in the present study because they are probably of second-order importance to advection as mechanisms of solute transport (see below). Here we utilize "full upstream weighting" in which the concentration of any species entering element l due to a flux is taken to be that of the upstream volume element. For an element l which has only one surface m over which upstream flow is entering we may write:

$$m_{i,l} = \frac{m_{i,up} F_{lm} \Delta t + m_{i,old}(V_{w,l} - F_{lm}\Delta t)}{V_{w,l}}, \tag{A4}$$

where $m_{i,l}$ = molality of species i in element l after advective mixing [moles/M], $m_{i,up}$ = molality of species i in the upstream element [moles/M], and $m_{i,old}$ = molality of species i in element l prior to advective mixing [moles/M]. An analogous expression may be formulated for any boundary flux F_{lb}.

Ideally, the mixing process should influence the entire volume element over a given interval of time Δt. However, in an explicit formulation, the solution will be characterized by unstable oscillations if the time step exceeds a critical limit (Rasmuson et al., 1982), definable for each element, which in the case of purely advective fluxes under steady flow conditions is given by:

$$\Delta t_{max} = \frac{V_{w,l}}{\sum^{upstream} F_l}. \tag{A5}$$

Physically, this expression states that the maximum stable time step is given by the ratio of the volume of water within l to the sum of all advectances entering from upstream volume elements across the boundaries of l. The time step over which coupled fluid flow and

chemical reaction occur is therefore constrained to be less than or equal to Δt_{max} which is in turn determined by the properties of the flow region. For the condition that fluid remains homogeneous in composition within a given volume element to be realistic, it is essential that the coupled fluid flow-chemical reaction time step approach Δt_{max}.

Utilizing the physical parameters and boundary conditions discussed in the text, we may evaluate the effects of neglecting molecular diffusion and mechanical dispersion. The relative importance of advection and molecular diffusion in a one-dimensional problem of constant volume element width Δy and uniform cross section may be investigated by defining the following Peclet number, Pe (Rasmuson et al., 1982):

$$Pe = \frac{V_f \Delta y}{2D}, \qquad (A6)$$

where V_f is the pore velocity, equal to the Darcy velocity divided by porosity, and D is the diffusivity of a solute species. Taking $V_f = 5 \times 10^{-8}$ m/s, $\Delta y = 1$ m, and D to be in the range of 10^{-9} to 10^{-12} m^2/sec (Freeze and Cherry, 1979), Pe ranges from about 25 to 25,000, illustrating the dominance of advection over diffusion.

The effects of mechanical dispersion may be as much as several orders of magnitude larger than those of molecular diffusion in advective systems (Garven and Freeze, 1984). The dispersive flux of solute species i across a surface segment $d\Gamma$ is given by:

$$J_{i,disp} = -n\alpha_L V_f \nabla c_{i,d\Gamma} \cdot n d\Gamma, \qquad (A7)$$

where $J_{i,disp}$ = rate of solute transport due to mechanical dispersion $[M/t]$, n = porosity, V_f = pore velocity [L/t], and α_L = longitudinal dispersivity [L].

For simplicity we consider here only the longitudinal component of dispersion which affects solute transport along the direction of fluid flow. An analogous expression for the advective flux, $J_{i,adv}$ can be derived from term (a) of equation (A1). In the supergene enrichment simulations, $\bar{c}_{i,d\Gamma}$ typically ranges from 0.1 to 100 moles/m^3 whereas $\nabla c_{i,l}$ approximated using finite differences, is on the order of 10^{-4} to 1 moles/m^3/m. The ratio $J_{i,adv}/J_{i,disp}$ gives an indication of the relative importance of the two processes in moving chemical species through the flow region. Using the values of $\bar{c}_{i,l}$ and $\nabla c_{i,l}$ discussed above and taking n = 0.12, $V_f = 5 \times 10^{-8}$ m/s, and a representative value for α_L of 1, the ratio of $J_{i,adv}/J_{i,disp}$ ranges from about 10 to 1,000 for a given interface $d\Gamma$.

In systems in which fluid flow rates are significantly slower and/or values of α_L are larger than those considered here, the effects of molecular diffusion and mechanical dispersion may be considerably more important. However, as a first approximation, we feel that neglect of molecular diffusion and mechanical dispersion in the relatively small, one-dimensional, and highly reactive flow system modeled here does not significantly alter any of the calculated geochemical systematics.

Chemical thermodynamics

Utilizing the EQ3NR/EQ6 computer programs of Wolery (1979, 1983), we have modeled the geochemical consequences of irreversible thermodynamics within the flow region, represented by term (b) of equation (A1). EQ3NR uses a modified Newton-Raphson algorithm to compute the equilibrium distribution of chemical species such as simple ions and aqueous complexes in an aqueous fluid. The input used by EQ3NR is a set of total concentrations of dissolved components or "aqueous master species" (Wolery, 1983) and some combination of pH, alkalinity, electrical balance, phase equilibrium, and redox state constraints necessary to define the equilibrium state of the fluid. EQ3NR must be used to provide the thermodynamic state of a fluid necessary to initialize an EQ6 simulation. EQ3NR, therefore, is a crucial link between calculations of advective solute transport using TRUST and the mixing procedure described above, and the computation of fluid-rock interaction performed by EQ6.

EQ6 utilizes the PATH approach developed by Helgeson et al. (1970) to compute fluid-rock interaction in closed systems. It does so using an algorithm employing Newton-Raphson iteration and finite differences. The computation scheme may be outlined as follows. The heterogeneous system on which EQ6 operates initially contains 1 kg of water of specified composition and a set of mineral reactants which are in general out of equilibrium with the aqueous phase. In response to this disequilibrium, mineral reactants dissolve which in turn perturbs the composition of the aqueous fluid. As reactants continue to dissolve, the fluid may become saturated with respect to one or more secondary mineral phases which are precipitated as the system attempts to attain a state of thermodynamic equilibrium. When an initial reactant reaches equilibrium with the fluid, dissolution of the reactant stops. The end state of the system is one in which either all remaining reactant phases have reached equilibrium with the fluid or all reactants have been destroyed.

In practice, EQ6 solves a highly nonlinear set of differential equations describing mass balance and mass action for the change in masses of all species within a heterogeneous system over each increment of reaction progress ξ (DeDonder and Rysselberghe, 1936; Helgeson, 1968). The rate R of a chemical reaction r may be related to the reaction progress ξ_r by:

$$R_r = \frac{d\xi_r}{dt}. \qquad (A8)$$

Thus the incorporation of mineral dissolution and precipitation rate laws into the solution procedure (cf. Delany et al., 1986) allows reaction progress to be translated directly into real time. In the present study mineral dissolution kinetics are modeled using a linear kinetic rate law (see text).

Because EQ6 operates on a system containing 1 kg of water, irreversible thermodynamic calculations in the context of coupled fluid flow and chemical reaction modeling require that moles of all minerals and their respective surface areas within a volume element l be normalized to correspond to the amount of rock which contains 1 kg of water. This is accomplished by dividing the total moles and surface area of each mineral within element l by the total fluid mass (in kg) of the element (Cunningham, 1984). This subvolume containing 1 kg of water is assumed to be a "representative elemental volume" which describes the geochemical characteristics of the entire volume element l.

The extension of EQ6 to an open system in which chemical reaction and solute transport are occurring requires consideration of mass balance within the flow region. In a system closed with respect to mass we may write for each chemical element e:

$$\frac{dn_{e,T}}{d\xi} = \sum_{\phi=1}^{NP} \gamma_{e,\phi} \frac{dn_\phi}{d\xi} + \sum_{s=1}^{NS} \gamma_{e,s} \frac{dn_s}{d\xi} + \sum_{rct=1}^{NR} \gamma_{e,rct} \frac{dn_{rct}}{d\xi} = 0, \quad \text{(A9)}$$

where e = chemical element in the system, $n_{e,T}$ = total number of moles of chemical element e in the system, n_k = number of moles of mineral phase or aqueous species where k = rct, s, or ϕ, NP = total number of secondary mineral phases, NR = total number of reactants, NS = total number of aqueous species, rct = denotes a reactant phase, s = denotes an aqueous species, $\gamma_{e,k}$ = number of moles of chemical element e in mineral phase or chemical species k, ϕ = denotes a secondary mineral phase, and ξ = reaction progress variable [moles]. Note that equation (A9) is here taken to describe mass balance in a rock volume containing 1 kg of water as required by EQ6. This mass balance constraint is applied as EQ6 computes reaction paths over any given coupled species transport-chemical reaction time step. After completion of this time step, new fluid fluxes are calculated and the advective mixing algorithm computes the new bulk fluid composition. Thus the total number of moles of chemical elements, $n_{e,T}$, have changed because a fluid with a different chemical composition has been advected into each volume element. The new total number of moles of a chemical element e, $n_{e,T,new}$, at the beginning of the next EQ6 calculation is:

$$n_{e,T,new} = \sum_{\phi=1}^{NP} \gamma_{e,\phi} n_\phi + \sum_{rct=1}^{NR} \gamma_{e,rct} n_{rct} \pm \sum_{s=1}^{NS} \gamma_{e,s} n_{s,new}, \quad \text{(A10)}$$

where $n_{s,new}$ is the new number of moles of species s after advective mixing within the reference rock volume containing 1 kg of water. The value of $n_{e,T,new}$ is then used in the first term of equation (A9) to provide the mass balance constraint for the next time step.

Program execution

The operation of the coupled fluid flow and chemical reaction program METASOM is depicted in Figure A1. TRUST, EQ3NR, and EQ6 have been incorporated into METASOM as a series of subroutines. Note that TRUST solves for fluid flow over all subvolumes simultaneously, whereas EQ3NR and EQ6 operate on one subvolume at a time. The problem is initialized with an EQ6 calculation which defines the chemical thermodynamic state of each volume element within the weathering profile before any fluid movement takes place. The program then enters the main loop in which computations of fluid flow and chemical reaction occur. The main loop begins with a calculation of fluid fluxes and other physical prop-

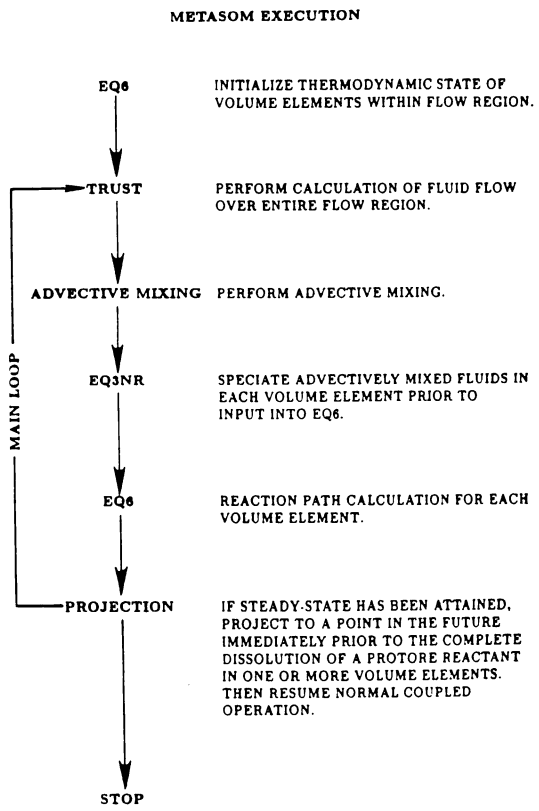

FIG. A-1. METASOM program execution procedure.

erties of the flow region such as saturation states. The computed fluid fluxes, in conjunction with the compositions of the aqueous phase within each volume element determined by EQ6, are then input into the advective mixing subroutines. The bulk composition of the advectively mixed fluid is in turn input into EQ3NR which performs the chemical speciations required by EQ6. Finally, EQ6 is called to calculate the water-rock interaction using the new fluid composition in each volume element.

This sequence repeats until either some specified maximum time is reached or the system displays steady behavior. In the latter case, the full set of equations describing fluid flow and chemical reaction do not have to be solved continuously. Instead, system behavior may be predicted simply by linear extrapolation of steady state flow rates and amounts of minerals precipitated and destroyed with time. Because this extrapolation results in a tremendous increase in execution efficiency and involves negligible loss of accuracy, we have incorporated an algorithm in the coupled fluid flow and chemical reaction program which, based on flow region behavior in steady state, computes the state of the system at some critically important point in the future. Here, these important points in the evolution of the weathering profile correspond to the complete dissolution of a given reactant phase, such as chalcopyrite, within one or more volume elements comprising the flow region. When a protore reactant dissolves completely from some part of the weathering system, normal coupled operation is resumed in order to compute in detail the geochemical consequences of reactant phase destruction. In this study, the criteria for steady state are met when fluid fluxes, fluid compositions, and amounts of reactant mineral dissolution and secondary phase precipitation are constant, within one percent, from one time step to the next. It should be noted that the steady state is attained only when steady fluid flow occurs within the weathering system and appropriate mineral dissolution kinetics expressions are utilized, as described within the paper.